• NASA Contractor Report 165935

NASA-CR-165935
19830001748

Interim Report

Analysis of Airfoil Leading Edge Separation Bubbles

J.E. Carter and V.N. Vatsa

UNITED TECHNOLOGIES RESEARCH CENTER
East Hartford, CT 06108

Contract NAS1-16585
May 1982

National Aeronautics and
Space Administration
Langley Research Center
Hampton, VA 23665

Analysis of Airfoil Leading Edge Separation Bubbles

TABLE OF CONTENTS

SUMMARY

A local inviscid-viscous interaction technique has been developed for the analysis of low-speed airfoil leading-edge transitional separation bubbles. In this analysis an inverse boundary-layer finite-difference analysis is solved iteratively with a Cauchy integral representation of the inviscid flow which is assumed to be a linear perturbation to a known global viscous airfoil analysis. Favorable comparisons with data indicate the overall validity of the present localized interaction approach. In addition numerical tests were performed to test the sensitivity of the computed results to the mesh size, limits on the Cauchy integral, and the location of the transition region.

INTRODUCTION

The classification of airfoil stall has been well known since the investigation of Jones (Ref. 1) in the early 1930's showed that there are three basic types of stall at subsonic speeds induced by trailing-edge separation and two types of leading-edge separation. Later the detailed experiments of McCullough and Gault (Ref. 2) revealed that trailing edge stall is associated with the separation of a turbulent boundary layer which moves forward with increasing incidence, leading-edge stall results from an abrupt separation of the laminar boundary layer near the leading edge without subsequent reattachment, and thin airfoil stall in which the laminar boundary layer separates near the leading edge followed downstream by turbulent reattachment which progresses rearward with increasing incidence. Further discussion on the classification of airfoil stall is presented in the excellent review article by Tani (Ref. 3).

In addition there has been recent work by van de Berg (Ref. 4) which indicates that leading-edge stall may not be the result of bursting of the laminar separation bubble, but rather it is due to separation of the turbulent boundary layer which develops downstream of this bubble. In this case it is still necessary, as pointed out by van den Berg, to be able to analyze the flow in the laminar separation bubble since it forms the initial conditions of the turbulent boundary layer downstream.

The focus of the present investigation is the development of a prediction technique for closed airfoil leading edge separation bubbles. It was pointed out by Tani (Ref. 3) that airfoils at moderate incidence angles, prior to either leading-edge stall or thin airfoil stall, experience local separation bubbles just downstream of the peak suction (minimum pressure) region. Figure 1 shows a schematic diagram of an airfoil leading-edge bubble which occurs if the Reynolds number is sufficiently low so that the boundary layer remains laminar up to the minimum pressure point. Downstream of this point separation occurs almost immediately since laminar boundary layers, in contrast with turbulent flows, are extremely sensitive to adverse pressure gradients. A separation bubble forms in which a recirculating streamline pattern is bounded by a shear layer. Since shear layer flows tend to be highly unstable to flow disturbances, transition from laminar to turbulent flow generally occurs in this shear layer. Further downstream the turbulent mixing between the shear layer flow with the lower dead air region results in entrainment of higher energy air which energizes the flow near the surface thereby resulting in flow reattachment with subsequent turbulent boundary-layer flow downstream. As shown in Fig. 1 the initial portion of the separation bubble is characterized by a pressure plateau followed by a pressure recovery region after the transition process is initiated, but prior to flow reattachment. An increase in incidence causes the bubble to move forward and contract in streamwise extent until the flow no longer reattaches. At this incidence angle bubble bursting has occurred, thereby resulting in leading-edge stall which is accompanied by an abrupt

loss of lift since the suction peak has now collapsed with the resultant pressure distribution redistributed in a flattened form over the airfoil chord.

There have been numerous experimental investigations conducted such as the work of Bursnall and Loftin (Ref. 5), Gault (Ref. 6), Gaster (Ref. 7), and more recently that of Mueller and Batill (Ref. 8) to provide information on the flow in the neighborhood of laminar transitional separation bubbles. Owen and Klanfer (Ref. 9) deduced from experimental measurements that bubble bursting occurs if the momentum thickness Reynolds number at the laminar separation point is less than 125; similarly, Crabtree (Ref. 10) proposed a criterion based on the pressure rise over the bubble. Later, Horton (Ref. 11) developed a semi-empirical theory based on the experimental measurements of Gaster (Ref. 7) for the growth and bursting of laminar separation bubbles. At the present time airfoil analysis codes such as the NASA-Lockheed multielement airfoil code (Ref. 12), and the GRUMFOIL code (Ref. 13) use simple criterions such as these to detect the occurrence of laminar separation bubbles and whether or not bursting occurs. In these analyses if laminar separation is detected without bursting then the flow is assumed to immediately undergo transition to turbulent flow with a jump discontinuity in the boundary-layer parameters such as shape factor and skin friction.

With the recent theoretical developments in boundary-layer and viscous-inviscid interaction theory for separated flow, there have been several analytical investigations (Refs. 14-18) conducted to provide a more detailed description of the flow process in a laminar separation bubble. These studies have been based on both finite-difference and integral techniques for describing the boundary-layer flow which are solved iteratively with a Cauchy integral representation of the inviscid flow. A particularly encouraging result was obtained by Briley and McDonald (Ref. 14) in which they showed that solutions obtained with viscous-inviscid theory were essentially the same as solutions obtained with the more computationally expensive Navier-Stokes equations.

The overall objective of the present investigation is the development of an analytical procedure for predicting airfoil leading-edge laminar separation bubbles. Prior to bursting, the streamwise extent of the separation bubble is only a few percent chord; hence, in a manner similar to the previous theoretical approaches discussed above, a local viscous-inviscid interaction analysis has been developed for the immediate vicinity of the separation bubble. However, in contrast with these previous efforts, the present perturbation approach is based on the use of a global airfoil viscous analysis which provides the reference pressure and displacement thickness as input for the local leading-edge interaction analysis. In this manner the global flow field around the airfoil, including the wake, is taken into account. In the present study the viscous airfoil analysis of Melnik, Chow and Mead (GRUMFOIL code, Ref. 13) has been used.

Computations are presented for several airfoils for which experimental data was available. In addition, comparison is made with the benchmark experimental data obtained by Gaster (Ref. 7). Overall the computed solutions are in good

agreement with the data, although it was observed that the solutions are quite sensitive to the transition model as will be demonstrated in the present report. Since the major thrust of the present work was to demonstrate the feasibility of a local interaction model used in conjunction with a global airfoil analysis, a simple streamwise intermittency function has been used to represent the transition from laminar to turbulent flow.

SYMBOLS

c	airfoil chord
c_f	skin friction coefficient
$\tilde{f}$	perturbation stream function
F	velocity ratio, u/u_e
g	total enthalpy ratio, H/H_e
H	total enthalpy
L	reference length
M	Mach number
m	perturbation mass flow
n	coordinate normal to reference displacement surface
N	coordinate measured normal to reference displacement surface from the body surface
Pr	Prandtl number
Pr_t	turbulent Prandtl number
q	perturbation source strength per unit length
Re	reference Reynolds number
Re_θ	local momentum thickness Reynolds number
s, S	coordinates along reference displacement surface
u	velocity component parallel to reference displacement surface
v	velocity component normal to reference displacement surface
V	transformed normal velocity in Prandtl transposition theorem
β	pressure gradient parameter
γ	streamwise intermittency function

δ^* displacement thickness

ε eddy viscosity coefficient

η transformed normal coordinate

μ molecular viscosity coefficient

ξ transformed tangential coordinate

ρ density

ψ stream function

Subscripts

e edge of boundary layer

I inviscid

ref reference solution

t_1 start of transition

t_2 end of transition

v viscous

∞ free stream

1 start of interaction region

2 end of interaction region

Superscripts

' perturbation quantity

i global viscous-inviscid iteration counter

VISCOUS-INVISCID INTERACTION ANALYSIS

The approach taken in the present effort to develop a prediction technique for airfoil leading-edge separation bubbles is based on a viscous-inviscid interaction technique in which the boundary-layer equations are solved iteratively with an inviscid analysis through displacement thickness coupling. As mentioned in the Introduction, the focus of the current effort is the analysis of closed transitional separation bubbles which are known from the experimental studies cited previously to occupy only a few percent of the airfoil chord. Since the resultant interaction is highly localized, it was decided to treat the leading-edge transitional bubble problem as a linear perturbation to a known global airfoil solution. The use of a localized interaction analysis, despite the overall approximation inherent in a perturbation approach, permits an accurate analysis of the flow field structure in this region, in contrast with the extremely difficult problem of trying to resolve this small scale phenomena while simultaneously solving the global airfoil flow field. However, the present approach, in contrast with previous perturbation treatments of this problem, accounts for the influence of the global viscous airfoil flow on the local interaction analysis. It is well known that at high angles of attack, where transitional bubbles frequently occur, the turbulent interaction at the airfoil trailing edge and wake influence the entire airfoil pressure including the location of the stagnation point and the level of suction pressure, which are the flow conditions upstream of the transitional bubble. In the present investigation the GRUMFOIL viscous airfoil analysis, developed by Melnik, Chow, and Mead (Ref. 13), was used to establish the reference pressure and displacement thickness distributions which were then input to the local interaction analysis which is described in this section. The local inviscid analysis is discussed first followed by a brief description of the boundary-layer analysis and the iteration procedure used to couple these two analyses.

Inviscid Analysis

Since most of the available experimental data for transitional bubbles is for low speed flows, the present analysis was restricted to low speed flow for which Laplace's equation is the governing equation for the inviscid velocity potential, Φ. Since this equation is linear, solutions can be superimposed and hence the velocity potential is written as

$$\Phi = \Phi_{ref} + \phi' \tag{1}$$

where Φ_{ref} is the velocity potential obtained from the global airfoil analysis for the flow over the reference displacement surface, shown in Fig. 2, and ϕ' is the perturbation potential due to the local transitional bubble. In the present analysis the disturbance field is represented by a distribution of sources placed

along the reference displacement surface for which the solution for ϕ' can be expressed as

$$\phi'(s,n) = \frac{1}{2\pi}\int_{s_1}^{s_2} q(\xi)\,\log\left[(s-\xi)^2+n^2\right]^{1/2} d\xi \tag{2}$$

where q is the source strength per unit length and s and n are the coordinates along and normal to the reference displacement surface, respectively. Equation (2) is only an approximate solution since it assumes that the sources are distributed along a straight line, whereas near the airfoil nose the reference displacement surface, which closely follows the airfoil shape, is highly curved. However, since the interaction length is very short it is assumed that over the interaction region the reference displacement surface is a straight line and hence the surface curvature has been neglected in the present investigation.

The perturbation velocity components induced by the deviation of the interaction displacement surface, shown in Fig. 2, from the reference displacement surface, are given by,

$$u' = \frac{\partial \phi'}{\partial s} \qquad v' = \frac{\partial \phi'}{\partial n} \tag{3}$$

which can be rewritten in terms of the perturbation potential using Eq. (2):

$$u'(s,n) = \frac{1}{2\pi}\int_{s_1}^{s_2} q(\xi)\,\frac{(s-\xi)d\xi}{(s-\xi)^2+n^2} \tag{4}$$

and

$$v'(s,n) = \frac{1}{2\pi}\int_{s_1}^{s_2} q(\xi)\,\frac{n d\xi}{(s-\xi)^2+n^2} \tag{5}$$

The source strength q is deduced by the imposition of the surface boundary condition which requires that the inviscid flow be tangent to the interaction displacement surface shown in Fig. 2. This boundary condition is given by

$$v'(s,\delta^*) = u(s,\delta^*)\,\frac{d(\delta^*-\delta^*_{ref})}{ds}\,\frac{1}{h(s,\delta^*)} \tag{6}$$

where

$$u = u_{ref} + u' \tag{7}$$

and

$$h = 1 + \kappa n \tag{8}$$

where κ is the curvature of the reference displacement surface which was set to zero in the present investigation. The boundary condition given in Eq. (6) can be transposed to the reference displacement surface by a Taylor series expansion and application of the continuity equation which results in

$$v'(s,o) = \frac{d\left[u_e(\delta^* - \delta^*_{ref})\right]}{ds} + o(\delta^* - \delta^*_{ref})^2 \tag{9}$$

where

$$u_e(s) = u(s,o) = u_{ref}(s,o) + u'(s,o) \tag{10}$$

The source strength is deduced by taking the limit of Eq. (5) as $n \to 0$ and the use of Eq. (9) which leads to

$$q(s) = 2v'(s,o) = 2\,\frac{d\left[u_e(\delta^* - \delta^*_{ref})\right]}{ds} \tag{11}$$

The final result needed for the present viscous-inviscid interaction calculations is the Cauchy integral for u'(s,o) which is obtained by the substitution of Eq. (11) into Eq. (4) which gives

$$u'(s,o) = \frac{1}{\pi}\int_{s_1}^{s_2} \frac{\frac{d}{d\xi}\left[u_e(\delta^* - \delta^*_{ref})\right] d\xi}{s - \xi} \tag{12}$$

with the total velocity $u_e(s)$, which is tangent to the interacted displacement surface, deduced from Eq. (10).

The Cauchy integral given in Eq. (12) is evaluated from s_1 to s_2 which is the region of strong interaction that results from the presence of the local transitional separation bubble. In the present calculations the reference displacement surface is computed from the GRUMFOIL analysis in which instantaneous transition from laminar to turbulent flow is assumed to occur at the predicted laminar separation point.

As a result the interaction displacement surface merges smoothly with the reference displacement surface upstream of the interaction as shown in Fig. 2. Hence the lower limit, s_1, on the Cauchy integral is placed sufficiently far upstream of the interaction region where the source strength is zero. The placement of the downstream limit is somewhat more complicated since the interacted displacement surface does not merge into the reference displacement surface downstream of the interaction region. This result is expected since the presence of the transitional separation bubble results in a thicker downstream turbulent boundary layer than that which is obtained with the GRUMFOIL analysis which eliminates the transitional separation bubble by placing transition at the laminar separation point. However it was found in the present calculations that the source strength is very close to zero downstream of the bubble since the interacted and reference displacement thicknesses are nearly parallel to each other. Numerical tests were performed which confirmed the insensitivity of the local interaction analysis to the values of the limits s_1 and s_2 provided they were placed sufficiently far enough upstream and downstream, respectively, of the interaction region. It is noted that the present perturbation procedure, which is based on the use of a reference displacement surface, considerably simplifies the choice of these limits over that used by other investigators in which the Cauchy integral was used to predict the disturbance field due to the total interaction displacement surface. In the latter case the reference solution is the inviscid flow over the airfoil.

The Cauchy integral given in Eq. (12) is evaluated numerically using a second-order scheme developed by Napolitano, et. al (Ref. 19). In this procedure the integration region, $s_1 \le s \le s_2$, is subdivided into I_{max} grid points with the complete integral written as the sum of integrals over these subintervals to yield the perturbation at the ith grid point:

$$u_i' = \frac{1}{\pi} \sum_{j=1}^{I_{max}-1} \int_{\bar{s}_{j-1}}^{\bar{s}_j} \frac{\frac{d}{d\xi}(u_e \Delta\delta^*)\, d\xi}{s_i - \xi} \tag{13}$$

where

$$\Delta\delta^* = \delta^* - \delta_{ref} \tag{14}$$

and

$$\bar{s}_j = \frac{s_j + s_{j+1}}{2} \tag{15}$$

With the source strength, $d/d\xi\ (u_e \Delta\delta^*)$ assumed to vary linearly over each subinterval, $\bar{s}_{j-1}$ to $\bar{s}_j$, Eq. (13) is analytically integrated to give

$$u_i' = \frac{1}{\pi} \sum_{j=1}^{I_{max}-1} \frac{d}{ds}(u_e \Delta\delta^*)\Big|_j \ln\left(\frac{s_i - \bar{s}_{j-1}}{s_i - \bar{s}_j}\right)$$

$$+ \frac{1}{\pi} \sum_{j=1}^{I_{max}-1} \frac{1}{\bar{s}_j - \bar{s}_{j-1}} \frac{d^2}{ds^2}(u_e \Delta\delta^*)\Big|_j \left[(s_i - s_j)\ln\left(\frac{s_i - \bar{s}_{j-1}}{s_i - \bar{s}_j}\right) - (\bar{s}_j - \bar{s}_{j-1})\right] \tag{16}$$

This numerical procedure permits the use of a nonuniform mesh distribution which was used in the present problem to concentrate grid points near the center of the interaction region in order to adequately resolve the high gradient phenomena which occurs as the flow undergoes transition from laminar to turbulent flow. The same surface grid point distribution was used in both the inviscid and boundary-layer analyses thereby avoiding interpolation between these two solutions in the interaction calculations.

Viscous Analysis

The viscous solution technique used in the present investigation is the inverse boundary-layer procedure presented by Carter (Ref. 20) for the analysis of separated flows. Although the inviscid analysis discussed in the previous section has been limited to low speed flow, the boundary-layer analysis used in the present study was adapted from earlier work which was for compressible flow. Thus the fully compressible boundary-layer analysis is presented here.

The nondimensional boundary-layer equations are written as follows in terms of the reference displacment surface coordinate system shown schematically in Fig. 2:

$$\frac{\partial \rho u}{\partial s} + \frac{\partial \overline{\rho v}}{\partial n} = 0 \tag{17}$$

$$\rho u \frac{\partial u}{\partial s} + \overline{\rho v} \frac{\partial u}{\partial n} = \rho_e u_e \frac{du_e}{dx} + \frac{\partial}{\partial n}\left[\mu \frac{\partial u}{\partial n} - \rho \overline{u'v'}\right] \tag{18}$$

$$\rho u \frac{\partial H}{\partial s} + \overline{\rho v} \frac{\partial H}{\partial n} = \frac{\partial}{\partial n}\left[\frac{\mu}{Pr}\frac{\partial H}{\partial n} - \rho \overline{v'H'} + \mu\left(1 - \frac{1}{Pr}\right) u \frac{\partial u}{\partial n}\right] \tag{19}$$

The v-component of velocity and the n-coordinate are scaled in the usual manner by $\sqrt{Re_{\infty,c}}$ where $Re_{\infty,c}$ is the Reynolds number based on the free stream flow conditions and the airfoil chord. The boundary conditions imposed on these governing equations are:

$$n = -\delta^*_{ref} \qquad u = v = 0, \quad H \text{ or } \frac{\partial H}{\partial n} \quad \text{specified} \tag{20}$$

$$n \to \infty \quad u \to u_e, \; H \to H_e \tag{21}$$

The Reynolds stresses are related to the mean flow by

$$-\rho \overline{u'v'} = \epsilon \gamma \frac{\partial u}{\partial n}, \quad -\rho \overline{v'H'} = \frac{\epsilon \gamma}{Pr_t} \frac{\partial H}{\partial n} \tag{22}$$

where ε is the eddy viscosity coefficient for which the Cebeci-Smith (Ref. 21) two-layer model for fully turbulent flows was used. The transition from laminar to turbulent flow was modeled by the use of a streamwise intermittency function $\gamma(s)$ which varies from 0 to 1 over a specified region. The treatment of the transition region will be discussed in more detail in the next section.

Werle and Verdon (Ref. 22) showed that it is convenient to transform the boundary-layer equations with the Prandtl transposition theorem which is given by

$$S = s, \quad N = n + \delta^*_{ref}, \quad V = v + u \frac{d\delta^*_{ref}}{ds} \tag{23}$$

where N is a transformed normal coordinate measured from the airfoil surface perpendicular to the reference displacement surface. In Ref. 22 it is shown that the form of the boundary-layer equations is unchanged by this transformation and the same surface boundary conditions (Eq. (20)) are imposed at N = 0.

The development of the inverse formulation begins by transforming the equations, expressed in primitive variables, by the following transformation of the independent variables

$$\xi = \int_0^x \rho_e \mu_e u_e \, ds \qquad \eta = \frac{1}{\delta^*} \int_0^N \frac{\rho}{\rho_e} \, dN \tag{24}$$

which is quite similar to the Levy-Lees transformation. It is helpful to scale the normal coordinate by the displacement thickness in strongly interacting flows since this step insures that the boundary-layer thickness is approximately constant in the transformed coordinate. The continuity equation is eliminated by introducing the stream function

$$\rho u = \frac{\partial \psi}{\partial N} \qquad \rho v = -\frac{\partial \psi}{\partial S} \tag{25}$$

The value of the stream function at the boundary-layer edge is written in terms of the displacement thickness

$$\psi \rightarrow \rho_e u_e (N - \delta^*) \tag{26}$$

where

$$\delta^* = \int_0^\infty \left(1 - \frac{\rho u}{\rho_e u_e}\right) dN \tag{27}$$

Then with the definitions

$$m = \rho_e u_e \delta^* \qquad h = \int_0^\infty \left(\frac{\rho_e}{\rho} - 1\right) d\eta \tag{28}$$

the edge value of the stream function can be written as

$$\psi \longrightarrow m\,(\eta - 1 + h) \quad \text{as} \quad \eta \longrightarrow \infty \tag{29}$$

A perturbation stream function is defined as

$$\tilde{f} = \frac{1}{\sqrt{2\xi}} \left[\psi - Fm\,(\eta - 1 + h)\right] \qquad \text{with} \quad F = \frac{u}{u_e} \tag{30}$$

such that $\tilde{f} \rightarrow 0$ as $\eta \rightarrow \infty$ for a prescribed m. Note that in the transformed inverse formulation the perturbation mass flow m is prescribed and not just the displacement thickness.

Transformation of the compressible boundary-layer equations with Eq. (24) and introduction of the perturbation stream function defined in Eq. (30) results in the following set of governing equations:

$$\frac{\partial \tilde{f}}{\partial \eta} = \frac{m}{\sqrt{2\xi}} (1 - \eta - h) \frac{\partial F}{\partial \eta} \tag{31}$$

$$m^2 F \frac{\partial F}{\partial \xi} - m \frac{\partial}{\partial \xi}\left[\sqrt{2\xi}\ \tilde{f} + mF(\eta - 1 + h)\right]\frac{\partial F}{\partial \eta} = \tag{32}$$
$$m^2 \beta (g - F^2) + \frac{\partial}{\partial \eta}\left[\left(1 + \frac{\epsilon}{\mu}\right) \ell \frac{\partial F}{\partial \eta}\right]$$

$$m^2 F \frac{\partial g}{\partial \xi} - m \frac{\partial}{\partial \xi}\left[\sqrt{2\xi}\ \tilde{f} + mF(\eta - 1 + h)\right]\frac{\partial g}{\partial \eta} = \tag{33}$$
$$\frac{1}{Pr} \frac{\partial}{\partial \eta}\left[\ell\left(1 + \frac{\epsilon}{\mu} \frac{Pr}{Pr_t}\right)\frac{\partial g}{\partial \eta}\right] + \frac{(\gamma - 1) M_e^2}{1 + \frac{\gamma - 1}{2} M_e^2} \frac{\partial}{\partial \eta}\left[\ell\left(1 - \frac{1}{Pr}\right) F \frac{\partial F}{\partial \eta}\right]$$

where

$$g = \frac{H}{H_e} \quad \beta = \frac{1}{M_e} \frac{dM_e}{d\xi} \quad \ell = \frac{\rho \mu}{\rho_e \mu_e} \tag{34}$$

Equations (31) - (33) are solved for F, g, $\tilde{f}$ and β for a prescribed streamwise distribution of m subject to the following boundary conditions:

$$\left.\begin{array}{l} \eta = 0 \quad F = \tilde{f} = 0 \quad g = g_w \ \text{ or } \left.\dfrac{\partial g}{\partial \eta}\right|_w \text{ specified} \\ \eta \to \infty \quad F = g \to 1 \ \text{ and } \ \tilde{f} \to 0 \end{array}\right\} \tag{35}$$

These equations can also be solved in the direct mode with β prescribed and the outer boundary condition $\tilde{f} = 0$ eliminated. In this case if m is set equal to $\sqrt{2\xi}$ then the usual Levy-Lees formulation is deduced with the only difference being that the normal component of velocity has been re-expressed in terms of the stream function. In the inverse case the unknown pressure gradient parameter is deduced simultaneously with the remainder of the solution. The numerical solution of these equations for both the direct and inverse mode is an implicit finite-difference technique which is first-order accurate in the stream direction and second-order accurate in the normal direction. The details of the numerical scheme are presented in Ref. 23.

Transition Model

The prediction of the transition process as a flow changes from laminar to turbulent remains one of the most challenging problems in fluid dynamics despite the enormous attention given this problem over the past sixty years. The prediction of transition is particularly difficult in the airfoil leading edge separation bubble since it occurs in a region where the viscous flow is strongly interacting with the local inviscid flow. To the author's knowledge, there have been only a few limited efforts, such as the work of van Ingen (Ref. 24), which have attempted to analyze the instability process which leads to transition from laminar to turbulent flow in a separated shear layer bounding a closed recirculation region. Since the objective of the present investigation was the development and demonstration of a viscous-inviscid interaction method for the analysis of airfoil leading edge transitional separation bubbles, a simple forced transition model in which the onset and length of transition were prespecified was used to obtain the results presented in this report. This model is described in this section along with a brief discussion of several attempts that were made in the early part of this investigation to use several existing semi-empirical natural transition models.

The forced transition model used in the present analysis is based on the streamwise intermittency distribution which was established by Dhawan and Narasimha (Ref. 25) by correlating a number of experimental studies of flows undergoing transition. This intermittency function is written as

$$\gamma = 1 - \exp\left[-0.412\left(\frac{s - s_{t_1}}{\lambda}\right)^2\right] \tag{36}$$

where s_{t_1} is the streamwise position where transition begins and

$$\lambda = s\Big|_{\gamma=0.75} - s\Big|_{\gamma=0.25} \tag{37}$$

The function γ, which multiplies the turbulent eddy viscosity as shown in Eq. (22), varies form 0 to 1 as the flow undergoes transition from laminar to fully turbulent flow. It was found to be convenient to express λ in Eq. (36) in terms of the location s_{t_2}, which is the end of transition and was assumed to occur at $\gamma = .99$. With this modification, Eq. (36) becomes

$$\gamma = 1 - \exp\left[-4.65\left(\frac{s - s_{t_1}}{s_{t_2} - s_{t_1}}\right)^2\right] \tag{38}$$

In the present calculations, the values of s_{t_1} and s_{t_2} were deduced from the experimental data and input to Eq. (38) to complete the specification of $\gamma(s)$. The sensitivity of the computed results to the intermittency function is presented in the section on Results and Discussion.

In the early stages of this investigation, calculations were attempted using the semi-empirical methods of Granville (Ref. 26) and Michel (Ref. 27) to predict the onset of transition. However, it was found that the use of these natural transition models predicted the onset of transition much further downstream than that which occurred in the experiments of Gaster (Ref. 7) and Gault (Ref. 6) on laminar separation bubbles. The main difficulty in the use of these models for the Gaster and Gault cases is that the Reynolds numbers in these experiments ($Re \approx 2 \times 10^6$) are at the lower Reynolds number range for which these correlations were established for which the data was insufficient to establish an accurate correlation. In addition, these correlations are probably not applicable to the present study of separated flow since they were established for much milder adverse pressure gradients than those encountered in the present study.

Interaction Iteration Procedure

The present analysis is based on a viscous-inviscid iteration technique which was previously presented by Carter (Ref. 28) and is adapted to the present investigation as outlined in Fig. 3. This procedure, which has been referred to as a semi-inverse technique by LeBalleur (Ref. 29), combines an inverse boundary-layer technique with a direct inviscid analysis via the update procedure shown in Fig. 3. The key feature of this iteration procedure is the simple update formula

$$m^{i+1} = m^i \left[1 + \omega \left(\frac{u_{e_V}}{u_{e_I}} - 1 \right) \right] \tag{39}$$

which permits an inverse boundary-layer analysis to be directly linked to an inviscid analysis which accounts for displacement thickness effects. Note that for simplicity the update formula is shown in Fig. 3 with the relaxation factor, ω, set equal to one. This interaction iteration procedure, shown in Fig. 3, is general and has been used in several other studies (Refs. 16, 22, 30 and 34) in which a variety of inverse boundary-layer and direct inviscid solution procedures have been employed. It was found by Kwon and Pletcher (Ref. 16) that convergence could be accelerated by making several inner-loop passes through the Cauchy integral and the update formula with the boundary-layer prediction of the edge velocity, u_{e_V}, frozen at its current global iteration value. This technique was used in the present calculations with three inner-loop passes and was found to accelerate the global convergence rate by a factor of three with a 50% reduction in computer time as compared to calculations made without this inner iteration.

RESULTS AND DISCUSSION

The Cauchy integral and inverse boundary-layer analysis which are used to iteratively solve for the local interaction region near a transitional separation bubble were combined into a computer code referred to as ALESEP (Airfoil Leading Edge Separation). The code is set up to input the displacement thickness and pressure distribution for the reference solution about which the local interaction analysis is assumed to be a linear perturbation. In this section, the results obtained with this analysis are presented for laminar and transitional separated flow over a flat plate with a trough, and comparison is made with the experimental data of Gaster (Ref. 7), and Gault (Ref. 6) for transitional separation bubbles. The sensitivity of this interaction analysis to the transition model, Reynolds number, grid size, and limits on the Cauchy integral is demonstrated in these results. In all of these calculations, 100 grid points were placed nonuniformly across the boundary layer with the minimum step size adjacent to the wall prescribed so as to provide an adequate resolution of the high gradient turbulent boundary layer which occurs downstream of the separation bubble. These calculations were initiated with an assumed linear distribution of the total displacement thickness and were continued until the difference between u_{e_I} and u_{e_V} was less than 0.2%. In general about 20 global viscous-inviscid interaction iterations were required. In most cases, the calculations were performed with a relaxation factor of unity.

Flat Plate With Trough

The present analysis was verified by computing the laminar separated flow over a flat plate with a trough which was initially analyzed by Carter and Wornom (Ref. 32) followed later by Kwon and Pletcher (Ref. 16), Veldman (Ref. 33) and Davis and Werle (Ref. 34). Since the results from all of these analyses are in excellent agreement, this separated flow provides an excellent benchmark case by which to test a newly-developed low speed viscous-inviscid interaction analysis. In this case, the interaction analysis was used to treat the total displacement body and hence $u_{e_{ref}}$ and δ^*_{ref} were set equal to zero. The interaction region was assumed to occur in the region, $1.0 \leq x/L \leq 4.0$, with the trough centered at $x/L = 2.5$ as shown in Fig. 4(a). In this case, the arclength has been replaced in the interaction analysis by the Cartesian coordinate x since they are nearly equal for this shallow trough. The displacement thickness contribution to the Cauchy integral upstream and downstream of the interaction region was treated by assuming that in these regions $\delta^* \sim \sqrt{x}$. For this case, a streamwise mesh of 121 grid points was distributed over the interaction region with a constant step size of $x/L = 0.025$.

The results obtained with the present analysis for this case were found to be in excellent agreement with those obtained previously by Carter and Wornom (Ref. 31).

The results for the edge velocity, skin friction, and displacement thickness are shown in Fig. 4. In addition, results are presented which demonstrate the effect of an imposed transition region, $2.35 \leq x/L \leq 2.55$, over which the intermittency factor was assumed to vary linearly from zero to one. In this case, the displacement thickness contribution to the Cauchy integral downstream of $x/L = 4$ was treated by assuming $\delta^* \sim x^{3/4}$. It is observed in Fig. 4 that the effect of including transition results in a smaller separation bubble and displacement thickness than that obtained in the completely laminar case. As a result, the edge velocity distribution in the transitional case more closely resembles the inviscid distribution shown in Fig. 4(a) since the overall interaction has been reduced in magnitude. Figure 4(b) shows that the skin friction has a rapid decrease at the start of transition followed by a rapid increase as the wall flow is energized due to turbulent mixing. This feature was observed in all transitional cases analyzed in the present investigation.

Gaster Experiment

Gaster (Ref. 7) performed a detailed experimental investigation on transitional separation bubbles which were induced on a flat plate by the pressure distribution which resulted from an airfoil placed near the plate. The particular case chosen from the Gaster data set for comparison with the present analysis is denoted in the Gaster report (Ref. 7) as Series I, number IV. The perturbation technique described in the analysis section was used in this calculation with the reference pressure, shown in Fig. 5(a), set equal to that measured by Gaster with the boundary layer tripped from laminar to turbulent flow near the flat plate leading edge. The reference displacement surface was computed from a direct calculation of the present finite-difference boundary-layer procedure with the reference pressure distribution prescribed and instantaneous transition assumed at the experimental trip location.

In the viscous-inviscid interaction calculation, a streamwise mesh of 81 grid points was distributed in the interaction region, $0.5 \leq s/L \leq 1.5$, with a constant step size of $\Delta s/L = 0.0125$. In this particular case, the best agreement of the computed results with the experimental data was obtained with transition assumed to occur instantaneously at $s/L = 1.0$. Figure 5 shows the predicted results for pressure, skin friction, displacement thickness, momentum thickness Reynolds number, and velocity profiles at various streamwise locations. Figure 5(a) shows excellent agreement between the computed pressure distribution and that obtained by Gaster for this transitional separation bubble. The localized nature of this interaction is evident in Fig. 5(a) since the transitional pressure distribution merges smoothly with the turbulent or reference pressure distribution upstream and downstream of the strong interaction region. It is observed in Fig. 5(a) that the presence of the transitional separation bubble slightly reduces the suction peak and results in a pressure plateau further downstream in the separated flow region. The "break" in the pressure curve occurs at the point where the flow was assumed to undergo instantaneous transition with a rapid recovery in pressure taking place immediately downstream. Figures 5(b) and 5(c) show excellent agreement in the predicted and

measured separation and reattachment points and the momentum thickness Reynolds number at the separation point, respectively. It is observed in Figs. 5(b) and 5(c) that just downstream of transition, a simultaneous decrease in the displacement thickness and an increase in the momentum thickness occurs which results in a rapid decrease in the shape factor, $H = \delta^*/\theta$. In many airfoil analyses, the transitional separation bubble is treated in an approximate manner by assuming the shape factor decreases discontinuously at the laminar separation point as transition from laminar to turbulent flow takes place. This approximate treatment of the transition region allows the analysis to continue without divergence due to the presence of separation; however, the details of the transitional separation bubble are completely missed with this approximation.

Figure 5(d) shows some of the velocity profiles computed in this case which illustrate the significant changes which occur in the shape of the profile over the interaction region. These profiles have only been plotted out to the n-location where $u/u_e = 0.995$ in order to show the large streamwise growth which occurs in the boundary-layer thickness as the transition process takes place.

Numerical tests were performed to test the sensitivity of the interaction analysis to the specification of the transition region. Figure 6(a) shows the two intermittency distributions which were used in these calculations along with the instantaneous transition model that was used in the results previously discussed. For the case designated as "small transition region" the Dhawan and Narasimha intermittency function given in Eq. (38) was used with $s_{t_1} = 0.9395$ and $s_{t_2} = 1.158$; in the case referred to as "large transition region", the start and end of transition were specified by $s_{t_1} = 0.958$ and $s_{t_2} = 1.271$, respectively. Figures 6(b), 6(c), and 6(d) show the effects of the different transition regions on the computed pressure, skin friction, and displacement thickness, respectively. These results show only small differences between the instantaneous and small transition region calculations; however, the computed interaction results differ significantly with the use of the intermittency distribution in the large transition region case. In this case, the onset of transition is delayed and the length scale of the transition region is increased as compared to the other two cases which results in a significant overprediction of the extent of the separated flow as shown in Figs. 6(b), 6(c), and 6(d). Although the large transition region model is not applicable to this particular case, the computed results show the correct qualitative behavior that would occur if transition were delayed due to a decrease in Reynolds number. Figure 6(b) shows that the presence of the large separation bubble reduces the pressure suction peak; the pressure plateau, characteristic of separated flows, is much more pronounced in this case. Even though the displacement thickness is much larger in this case, the local interaction model is still applicable since the pressure merges smoothly upstream and downstream with the reference pressure distribution shown in Fig. 5(a). Although not presented here, results were also obtained with the imposed transition region moved further upstream near the laminar separation point. As expected, these results show a significant underprediction in the extent of the separation bubble and subsequent interaction. It is concluded from this study that the use of the Dhawan

and Narasimha intermittency function in the present interaction analysis produces physically correct results; however, further work is clearly required in order to obtain an analytical procedure which provides the onset and length of the transition region.

A brief numerical study was also conducted to determine the effect of the streamwise mesh size on the computed results. Three calculations were made for the case which utilized the small transition region with the grid spacings of $\Delta s/L = 0.025$, 0.0125, and 0.00625. Figure 7(a) shows the skin friction deduced in these calculations in which it is observed that the results show only minor differences due to the change in the grid size. More sensitivity is observed in the computed displacement thickness shown in Fig. 7(b) in which noticeable changes occur downstream of the transition region for the different grid spacings which were used. The first order accuracy of the boundary-layer finite-difference scheme is apparent in Fig. 7(b) since the differences between the solutions vary in an approximately linear manner with the size of the grid spacing. Despite these differences in the displacement thickness, the computed pressure was essentially the same for all three grid sizes. In the future, if it is considered necessary, a second-order scheme could be utilized to achieve a more rapid convergence rate of the solution with decreasing mesh size. Alternately, as has been done in the remainder of the calculations, a variable grid can be used with the smallest grid spacings placed in the transition region to minimize the truncation errors associated with this high gradient region.

Gault NACA 66_3-018 Airfoil

Gault (Ref. 6) made detailed experimental measurements of transitional bubbles on different airfoils at various flow conditions. In the remainder of this report, several comparisons are made with this data using the present localized interaction analysis. In the first case, an analysis was conducted for the transitional bubble which occurs at the leading edge of a NACA 66_3-018 airfoil at a chord Reynolds number of 1.5×10^6 and 12 degrees angle of attack. At this angle of attack, the reference solution, obtained from the GRUMFOIL code (Ref. 13), was found to significantly overpredict the lift coefficient reported by Abbott and von Doenhoff (Ref. 35) for this airfoil. Correspondingly, the pressures in the strong acceleration region were overpredicted thereby providing an inaccurate reference solution for this case. These errors are probably due to the inability of the GRUMFOIL code to correctly model the lift decrement due to the massive trailing edge separation which occurred in this case at 0.75 chord on the upper surface. In order to compensate for this problem, the GRUMFOIL code was run at a reduced angle of attack of 11.25° which provided a much better match of the experimental lift coefficient and the pressure distribution between the stagnation point and the peak suction region as shown in Fig. 8(a).

The local interaction analysis was performed with a variable streamwise mesh of 78 grid points distributed over the interaction region - $0.0148 \leq s/c \leq 0.31$, where s is the arclength measured from the airfoil line of symmetry. In the present

case as well as the NACA 0010 (Modified) airfoil case to be discussed next, the arclength was measured along the actual airfoil surface instead of the reference displacement surface since these two surfaces are nearly coincident for these two cases. The transition region was imposed from $s_{t_1} = 0.0258$ to $s_{t_2} = 0.0432$ with the Dhawan and Narasimha intermittency function. The location of s_{t_1} was placed approximately midway between the separation point and the "break" point in the experimental pressure distribution; s_{t_2} was located so that the intermittency function gave a value of $\gamma = 0.5$ at the experimental pressure "break" point. With an assumed initial distribution of a linarly varying displacement thickness, it was found that the interaction calculation was unstable; however, this instability was eliminated and converged results were obtained in 50 global iteration cycles by using an underelaxation factor of 0.5 on the perturbation mass flow parameter, m, in each cycle of the global iteration procedure shown in Fig. 3.

The computed results for this case are shown in Figs. 8(a) and 8(b) for the pressure, and skin friction and displacement thickness, respectively. Good agreement is obtained between the predicted results and Gault's pressure data and measured separation point for this case. Figure 8(a) also shows the inviscid airfoil pressure distribution which was obtained from the GRUMFOIL code with $\alpha = 11.25°$. The large difference between this solution and the viscous airfoil solution obtained with the GRUMFOIL code shows the importance of including the viscous effects in the reference solution which is input to the present perturbation interaction analysis.

Two additional calculations were performed to test the sensitivity of the interaction analysis to the upstream and downstream limits on the Cauchy integral given in Eq. (12). In the first calculation, the lower limit was placed at $s_1 = 0$ with $s_2 = 0.31$ as was used earlier; in the second calculation, the upper limit was placed at $s_2 = 0.12$ with $s_1 = -0.0148$ as was used earlier. The results of these calculations resulted in no significant changes from those discussed previously, thereby verifying that in the present perturbation approach the numerical solution of the Cauchy integral can be confined to the interaction region. This point is further supported by Fig. 8(c) which shows the streamwise variation of the difference between the interacted and reference displacement thickness. Both upstream and downstream of the interaction region, the increment in the displacement thickness is nearly constant and thus provides virtually no contribution to the Cauchy integral source strength in these regions. It is observed in Fig. 8(c) that upstream of the interaction region, in the laminar portion of the flow, the displacement thickness increment differs slightly from zero, this small difference being due to the difference between the integral laminar boundary-layer analysis in the GRUMFOIL code and the present finite-difference approach.

Gault NACA 0010 (Modified) Airfoil

Calculations were performed for this airfoil, tested experimentally by Gault (Ref. 6), for an angle of attack of 8° and a chord Reynolds number of 2 and 4 x 10^6.

The reference viscous airfoil solution, obtained from the GRUMFOIL code, gave good agreement as shown in Figs. 9(a) and 9(b) with the experimental pressure distribution in the strong acceleration region ahead of the transitional separation buffle. In this case, the turbulent separation at the trailing edge was less than 1% chord thereby having no significant effect on the leading edge pressure distribution. In the interaction calculations, 71 grid points were distributed nonuniformly in the interaction region, $0 \leq s/c \leq 0.32$, with the minimum grid spacing placed in the transition region. The intermittency functions for these calculations, which are shown in Fig. 9(c), were prescribed in the same manner as those used in the NACA 66_3-018 airfoil calculations.

Comparison of the predicted pressure distributions and Gault's experimental data for $Re_c = 4 \times 10^6$ and 2×10^6 are shown in Figs. 9(a) and 9(b), respectively. Although the present analysis shows the same overall features as the data, the detailed agreement between the interacted solution and Gault's data is not as good as that shown earlier for the NACA 66_3-018 airfoil. In this case, the data has a local constant pressure region in the peak suction region which was not obtained in either the interaction solution or in the inviscid and reference solutions obtained from the GRUMFOIL analysis. A number of calculations were performed with different intermittency distributions to see if improved agreement could be obtained with the experimental data in the peak suction region. However, none of these assumed functions improved the agreement since this region is upstream of the separation bubble as shown by the skin friction distribution presented in Fig. 9(d). It is possible that this discrepancy arises due to the coarseness in the specification of the airfoil coordinates given by Gault for this modified NACA airfoil.

Comparison of the pressure distributions given in Figs. 9(a) and 9(b) shows that the onset of the adverse pressure gradient region, which leads to the separation bubble, occurs further upstream in the interaction solution than that observed experimentally by Gault. As a result, the present laminar separation point is predicted upstream of that measured by Gault as shown in Fig. 9(d) for the skin friction distribution. In addition, the present calculation overpredicts the length of the separation bubble since the point of reattachment was found to occur downstream of that measured by Gault. Despite these differences, the present analysis as shown in Fig. 9(d), predicts the correct Reynolds number effect on the airfoil leading edge separation bubble since the separation point moves only slightly for an increase in Reynolds number whereas the upstream movement of the reattachment point is by about the same amount as that found by Gault. Figure 9(e) shows the displacement thickness distributions for these two Reynolds numbers in which the upstream shift in the interaction region and the decreased magnitude of the displacement thickness are observed for the higher Reynolds number case. The pressure distributions are consistent with this result since the higher Reynolds number case shown in Fig. 9(a) has a shorter pressure plateau in the separated flow region than that for the lower Reynolds number case presented in Fig. 9(b).

CONCLUDING REMARKS

A local inviscid-viscous interaction technique has been developed for the analysis of low-speed airfoil leading-edge transitional separation bubbles. In this analysis an inverse finite-difference boundary-layer procedure is iteratively combined with a Cauchy integral representation of the inviscid flow which is assumed to be a locally linear perturbation to a known global viscous airfoil solution. In this report a number of comparisons have been made with experimental data for transitional separation bubbles. Overall, good agreement has been obtained in these comparisons which indicates the validity of the present local interaction technique. In contrast with existing global airfoil analyses, the present localized interaction analysis is demonstrated to be capable of resolving the details of leading-edge transitional bubbles which occupy only a few percent of the airfoil chord. In the future this interaction analysis should be applied over a wider range of flows to see if the correct Reynolds number and angle of attack effects on airfoil transitional separation bubbles can be predicted.

In these comparisons a forced transition model has been used in which the onset and length of the transition region was specified a priori. Numerical tests were performed with this model which indicated that the flow is somewhat sensitive to the specified transition region. Whereas the use of a forced transition model allowed the assessment of the overall interaction model presented herein, in the future work should be directed at the development of a natural transition model for the prediction of transitional separation bubbles.

REFERENCES

1. Jones, B. M.: An Experimental Study of the Stalling of Wings, A.R.C.R. & M. 1588, December 1933.

2. McCullough, G. B. and D. E. Gault: Examples of Three Representative Types of Airfoil Section Stall at Low Speed, NACA TN 2502, September 1951.

3. Tani, I.: Low-Speed Flows Involving Bubble Separations, Progress in Aeronautical Sciences, Vol. 5, Pergammon Press, 1964.

4. van den Berg, B.: Role of Laminar Separation Bubbles in Airfoil Leading Edge Stalls, AIAA J. Vol. 19, No. 5, pp. 553-556, May 1981.

5. Bursnall, W. J. and L. K. Loftin, Jr.: Experimental Investigation of Localized Regions of Laminar-Boundary-Layer Separation, NACA TN 233, April 1951.

6. Gault, D. E.: An Experimental Investigation of Separated Laminar Flow, NASA TN 3505, September 1955.

7. Gaster, M.: The Structure and Behavior of Laminar Separation Bubbles, AGARD Conference Proceedings 4, pp. 819-854, 1966.

8. Mueller, T. J. and S. M. Batill: Experimental Studies of the Laminar Separation Bubble on a Two-Dimensional Airfoil at Low Reynolds Numbers, AIAA Paper No. 80-1440, 1980.

9. Owen, P. R. and L. Klanfer: On the Laminar Boundary Layer Separation from the Leading Edge of a Thin Airfoil, Aeronautical Research Council, Britain, Current Paper 220, 1955.

10. Crabtree, L. F.: Effects of Leading Edge Separation on Thin Wings in Two-Dimensional Incompressible Flow, Journal of Aeronautical Sciences, Vol. 24, pp. 597-604, August 1957.

11. Horton, H. P.: A Semi-Empirical Theory for the Growth and Bursting of Laminar Separation Bubbles, Aeronautical Research Council, Britain Current Paper 1073, 1967.

12. Stevens, W. A., S. H. Goradia, and J. A. Braden: A Mathematical Model for Two-Dimensional Multi-Component Airfoils in Viscous FLows, NASA CR-1843, July 1971.

13. Melnik, R. E., R. Chow, and H. R. Mead: Theory of Viscous Transonic Flow Over Airfoils at High Reynolds Number, AIAA Paper No. 77-680, June 1977.

14. Briley, W. R. and H. McDonald: Numerical Prediction of Incompressible Separation Bubbles, J. Fluid Mechanics, Vol. 69, Part 4, pp. 631-656, 1975.

15. Crimi, P. and B. L. Reeves: Analysis of Leading-Edge Separation Bubbles on Airfoils, AIAA J. Vol. 14, No. 11, pp. 1548-1555, November 1976.

16. Kwon, O. K. and R. H. Pletcher: Prediction of Incompressible Separated Boundary Layers Including Viscous-Inviscid Interaction, J. Fluids Engineering, Vol. 101, pp. 466-472, December 1979.

17. Gleyzes, C., J. Cousteix, and J. L. Bonnet: Bulbe de Decollment Laminaire Avec Transition - Essai de Prevision Avec Coupleze Local, AGARD Conference on Computation of Viscous-Inviscid Interactions, No. 21, AGARD CP-291, October 1980.

18. Cebeci, T., K. Stewartson, and P. G. Williams: Separation and Reattachment Near the Leading Edge of a Thin Airfoil at Incidence, AGARD Conference on Computation of Viscous-Inviscid Interactions, No. 20, AGARD CP-291, October 1980.

19. Napolitano, M., M. J. Werle, and R. T. Davis: Numerical Solutions of the Triple-Deck Equations for Supersonic and Subsonic Flow Past a Hump, University of Cincinnati, Report No. AFL 78-6-42, June 1978.

20. Carter, J. E.: Viscous-Inviscid Interaction Analysis of Transonic Turbulent Separated Flow, AIAA Paper 81-1241, 1981.

21. Cebeci, T. and A. M. O. Smith: Analysis of Turbulent Boundary Layers, Academic Press, 1974.

22. Werle, M. J. and J. M. Verdon: Viscid Inviscid Interaction for Symmetric Trailing Edges, Naval Air Systems Command Contract Report N00019-78-C-0604, January 1980.

23. Carter, J. E.: Inverse Boundary Layer Theory and Comparison with Experiment. NASA TP-1208, September 1978.

24. Van Ingen, J. L.: Transition, Pressure Gradient, Suction Separation and Stability Theory, AGARD CP-224, Laminar-Turbulent Transition, May 1977.

25. Dhawan, S. and R. Narasimha: Some Properties of Boundary Layer Flow During Transition from Laminar to Turbulent Motion, J. Fluid Mechanics, Vol. 3, 1958.

26. Granville, P. S.: The Calculation of Viscous Drag of Bodies of Revolution, Navy Department, The David Taylor Model Basin, Report No. 849, 1953.

27. Michel, R.: Prediction of the Onset and Development of Boundary Layer Transition, ESA TT-414, October 1977.

28. Carter, J. E.: A New Boundary-Layer Inviscid Iteration Technique for Separated Flow, AIAA Paper No. 79-1450, AIAA 4th Computational Fluid Dynamic Conference, Williamsbury, VA, July 23-25, 1979.

29. LeBalleur, J. C.: Couplage Visqueux-Non Visquex: Methode Numerique et Applications Aux Ecoulements Bidimensionnels Transsoniques et Supersoniques, La Recherche Aerospatiale, No. 1978-2, pp. 65-76, 1978.

30. Kuhn, G. D.: An Improved Interaction Method for Exhaust Nozzle Boattail Flows, AIAA Paper No. 80-0197, January 1980.

31. Whitfield, D. L., T. J. Swafford, and J. J. Jacocks: Calculation of Turbulent Boundary Layers with Separation and Viscous-Inviscid Interaction, AIAA J. Vol. 19, No. 10, pp. 1315-1322, October 1981.

32. Carter, J. E. and S. F. Wornom: Solutions for Incompressible Separated Boundary Layers Including Viscous-Inviscid Interaction. Aerodynamic Analysis Requiring Advanced Computers, Part I, NASA Sp-347, pp. 125-150.

33. Veldman, A. E. P.: New, Quasi-simultaneous Method to Calculate Interacting Boundary Layers, AIAA J. Vol. 19, No. 1, pp. 79-85, January 1981.

34. Davis, R. T. and M. J. Werle: Progress on Interacting Boundary-Layer Computation at High Reynolds Number, Presented at Conference "Numerical and Physical Aspects of Aerodynamic Flows," held at California State University at Long Beach, January 19-21, 1981.

35. Abbott, I. H. and A. E. von Doenhoff: Theory of Wing Sections, Dover Publications, Inc., 1959.

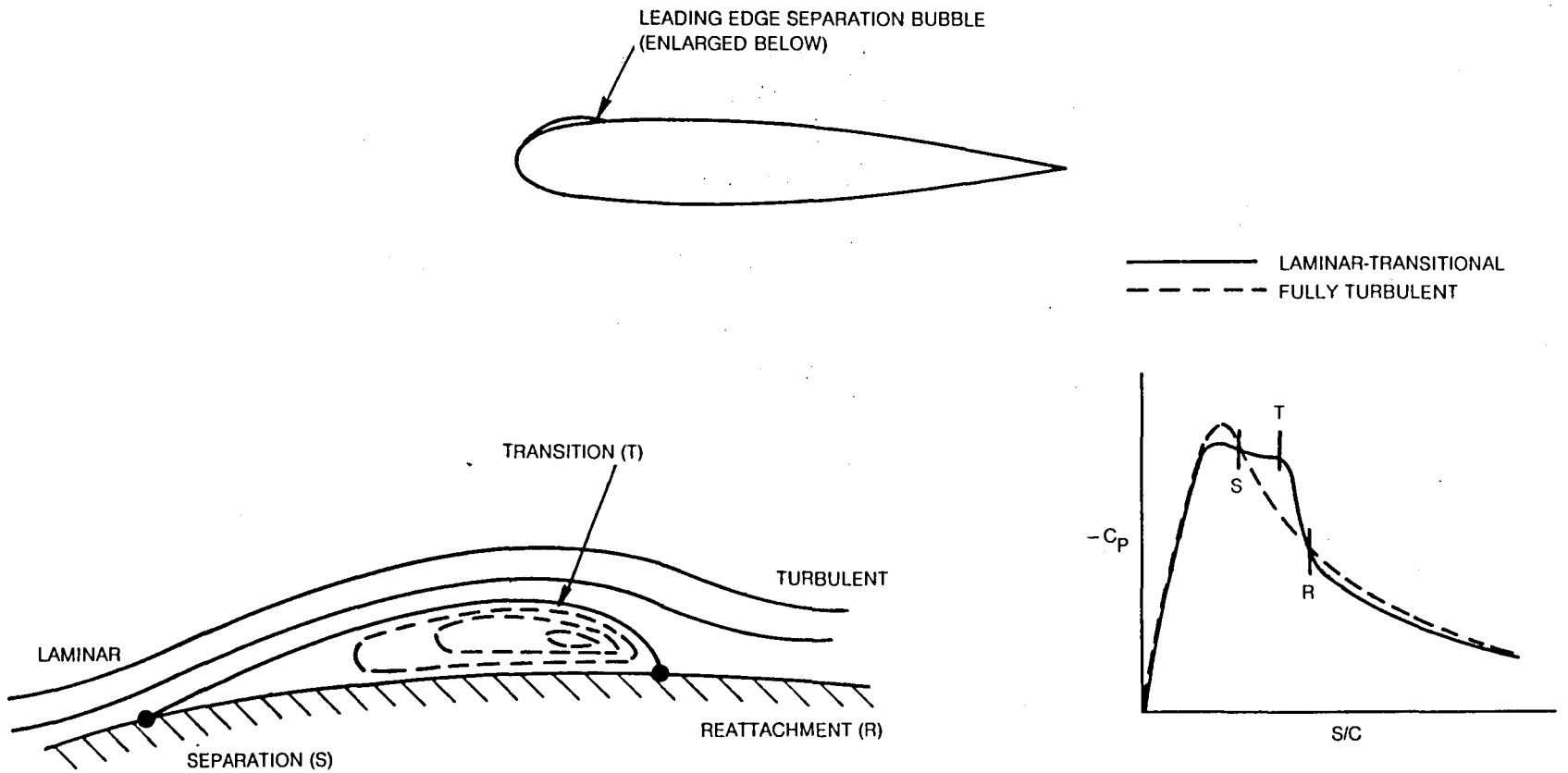

Fig. 1 Schematic diagram of airfoil laminar-transitional separation bubble and pressure distribution

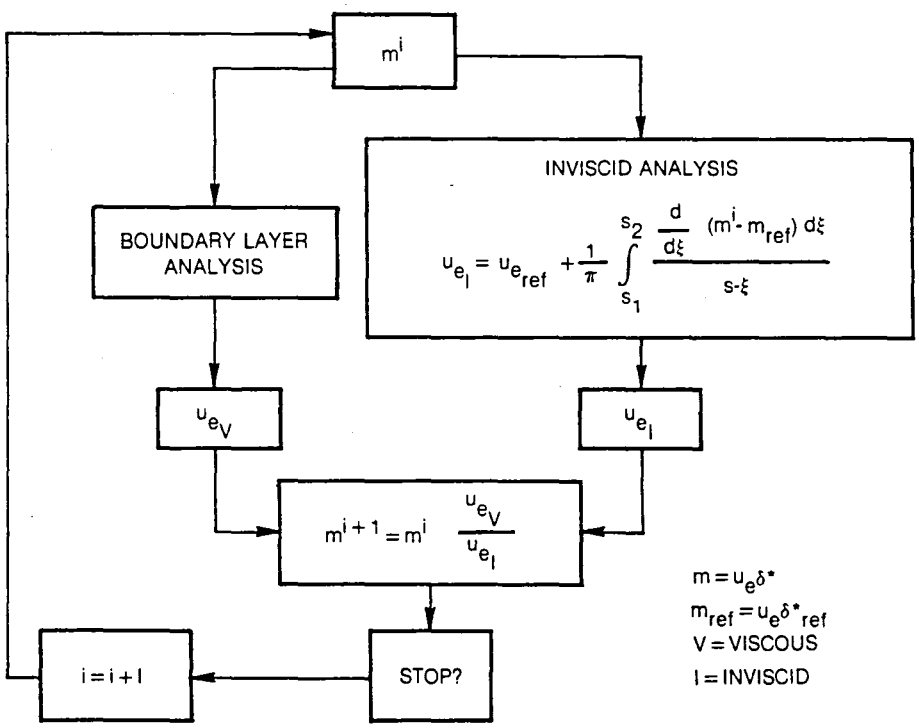

Fig. 3 Viscous-inviscid iteration procedure

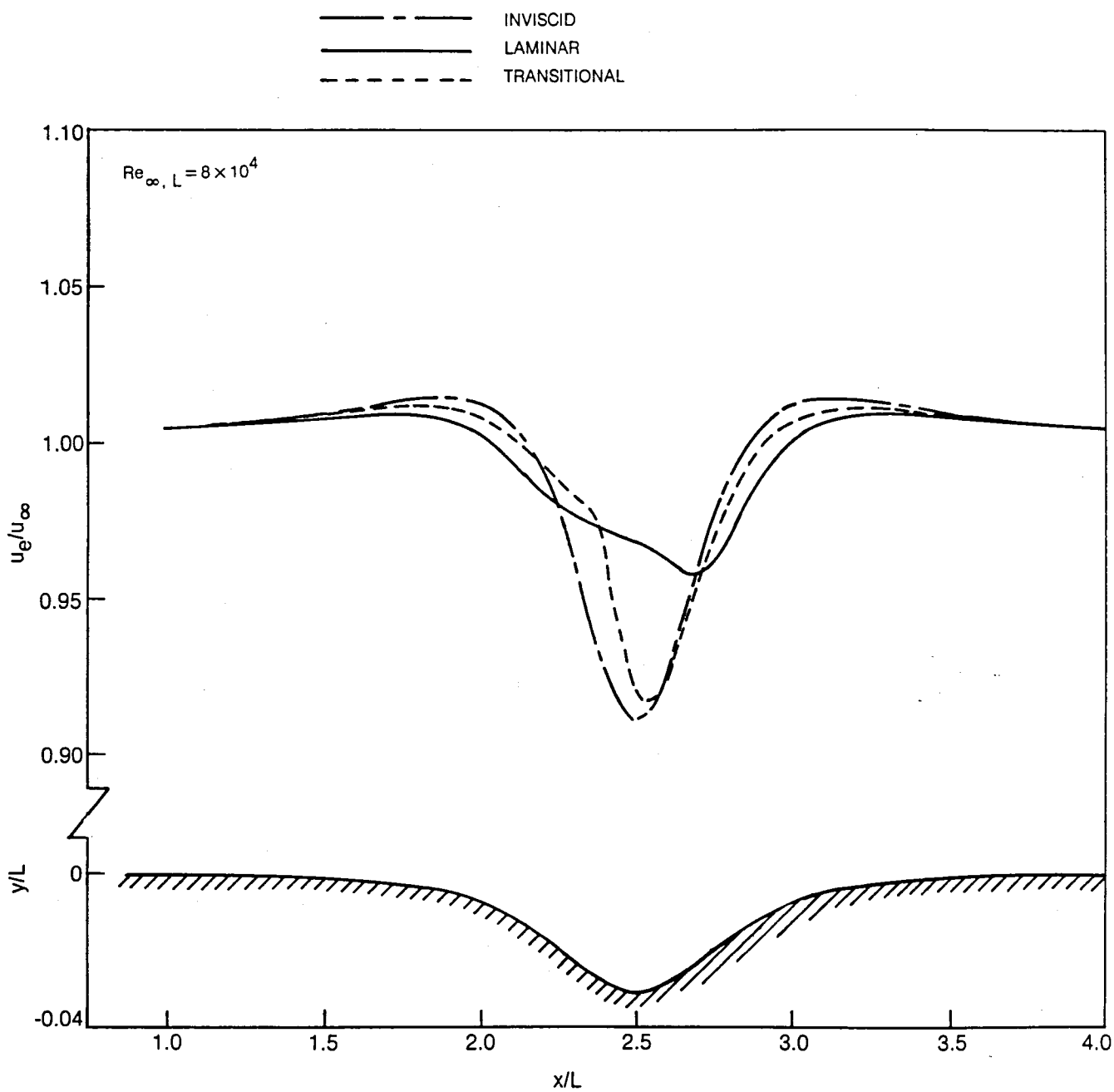

Fig. 4 Comparison of laminar and transitional separated flow results
a) Edge velocity and body shape

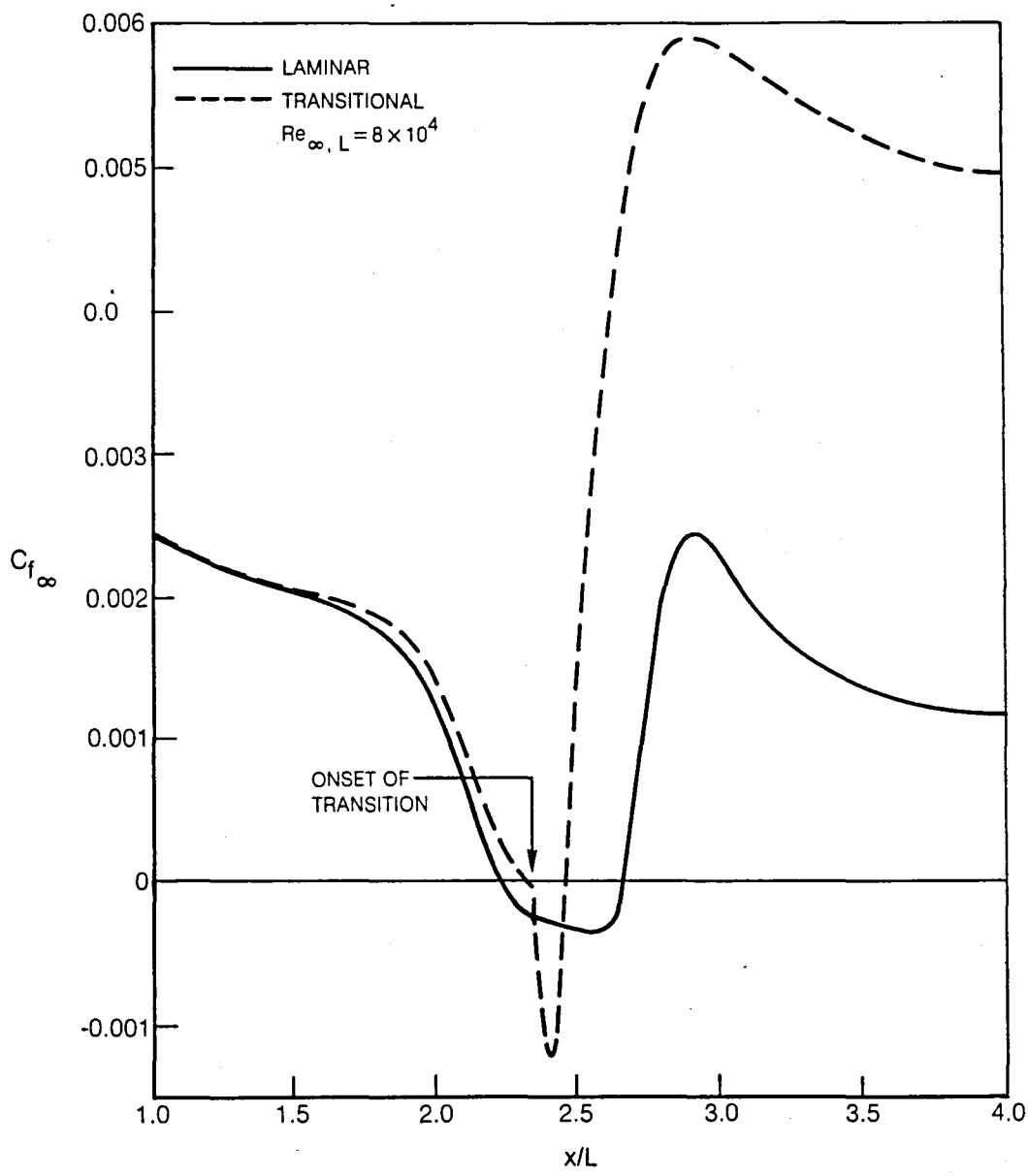

Fig. 4(b) Skin friction

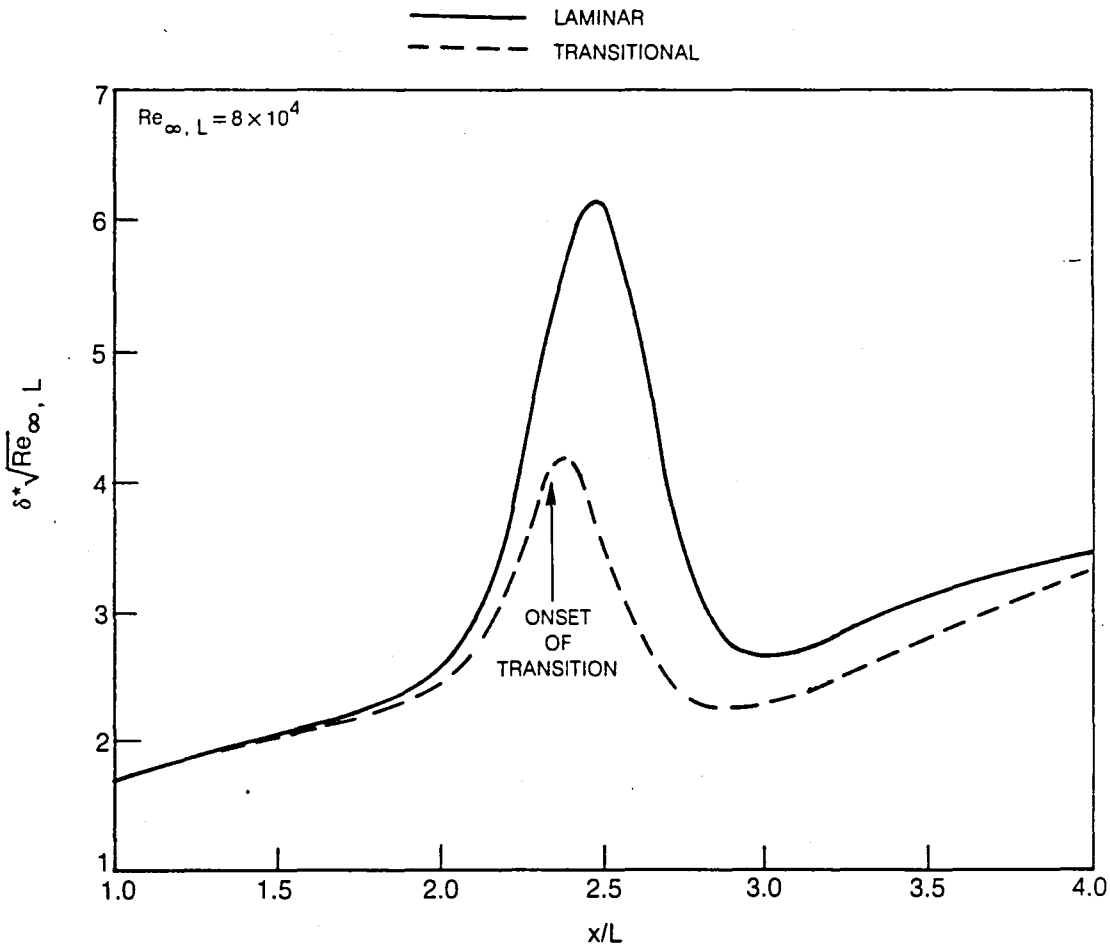

Fig. 4(c) Displacement thickness

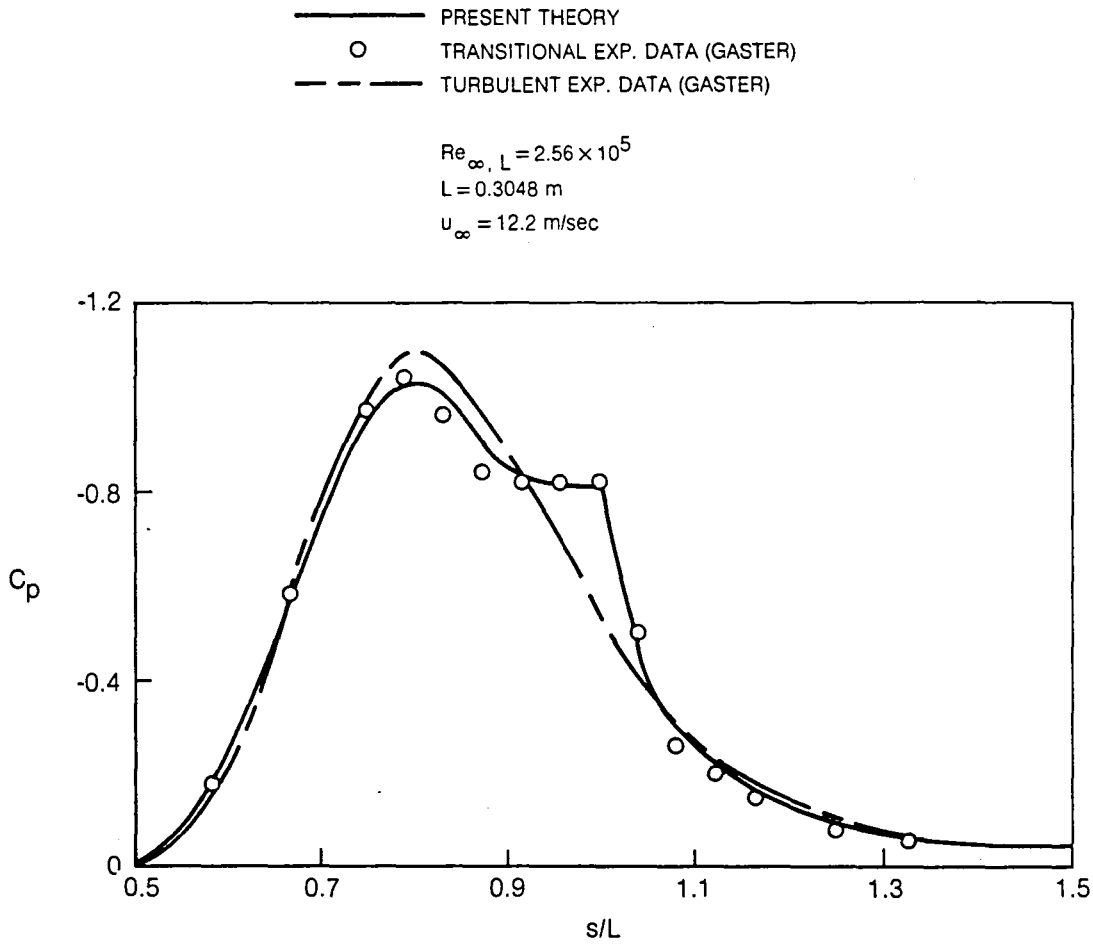

Fig. 5 Predicted results for Gaster case
a) Pressure

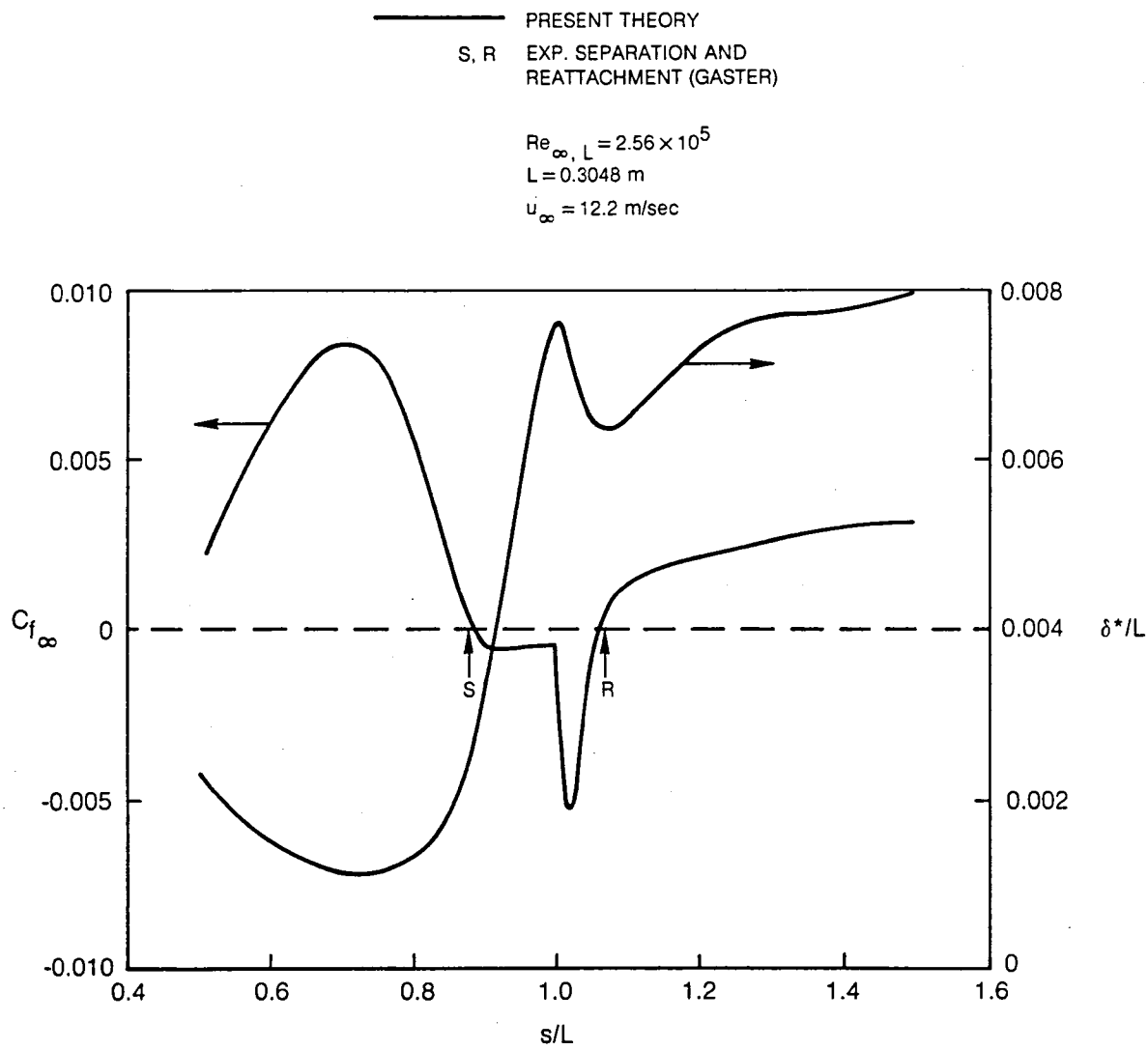

Fig. 5(b) Skin friction and displacement thickness

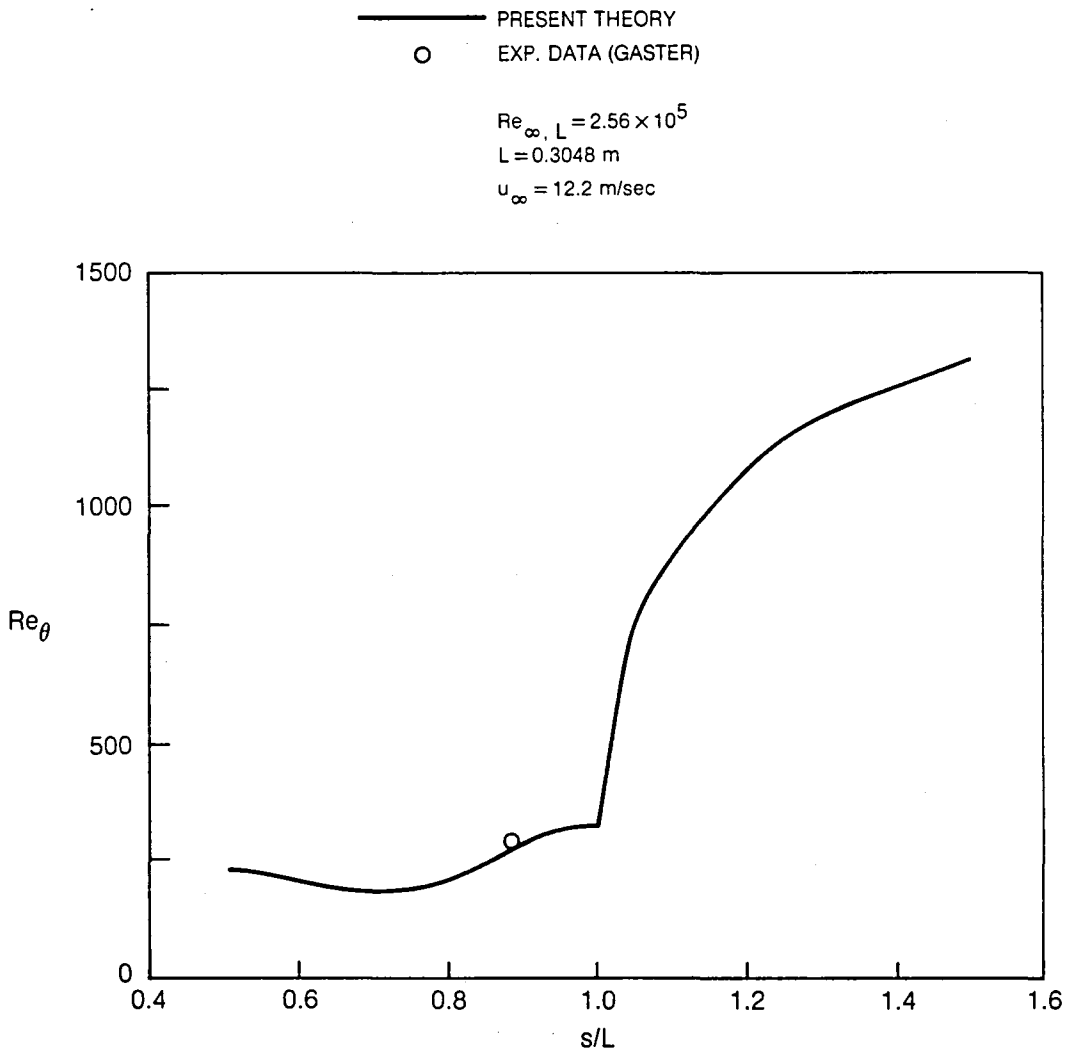

Fig. 5(c) Momentum thickness Reynolds number

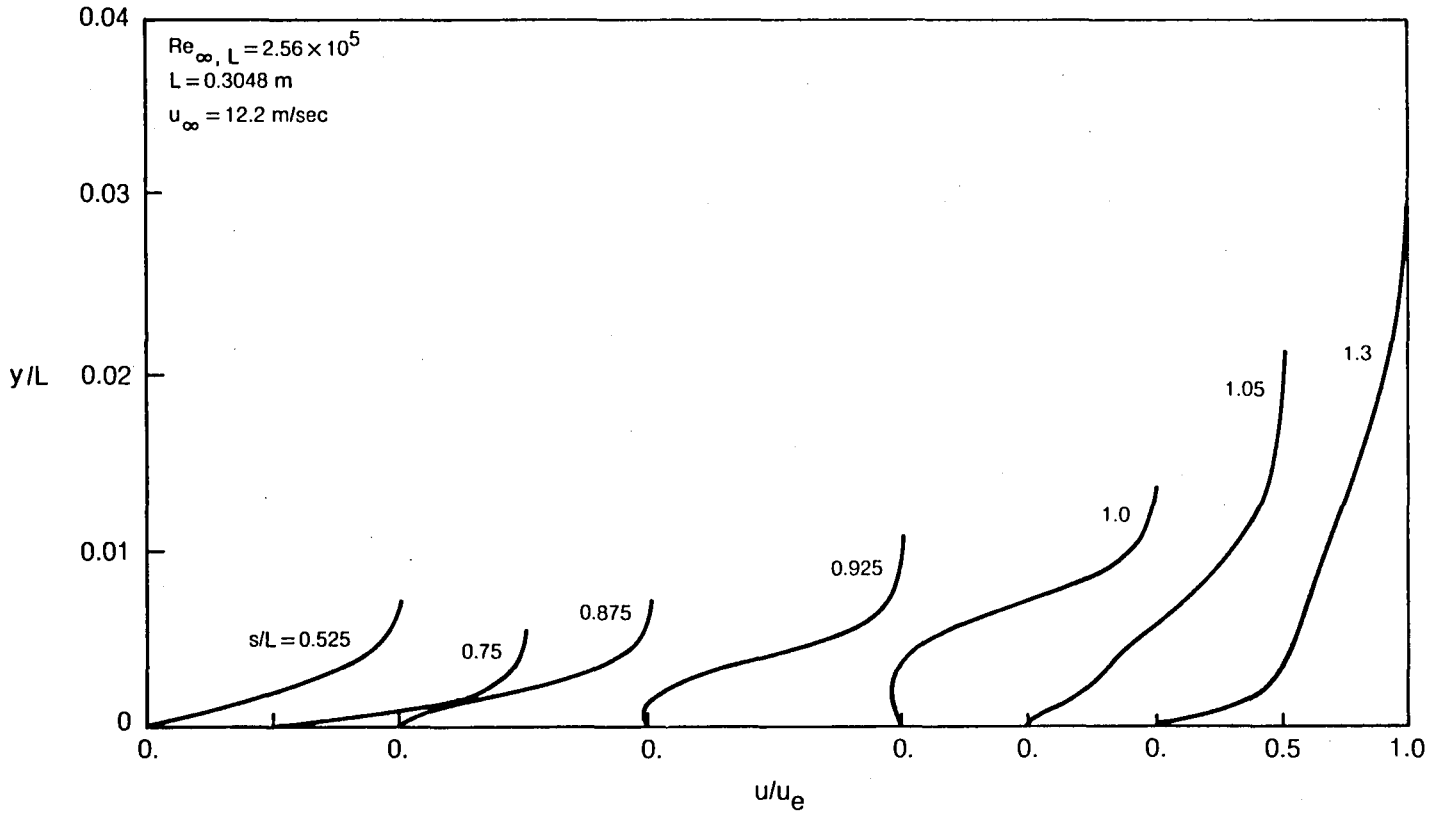

Fig. 5(d) Velocity profiles

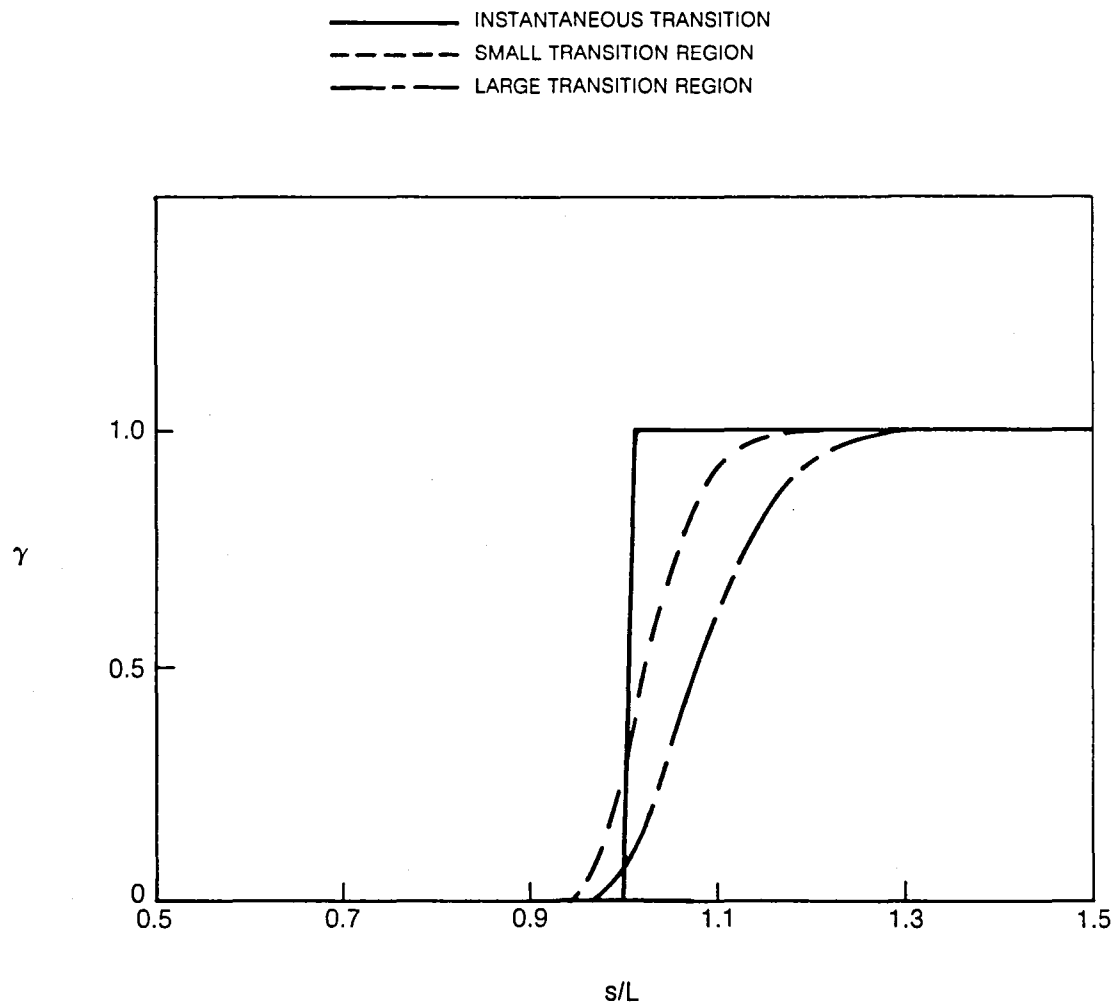

Fig. 6 Effect of transition region on predicted results
a) Intermittency function

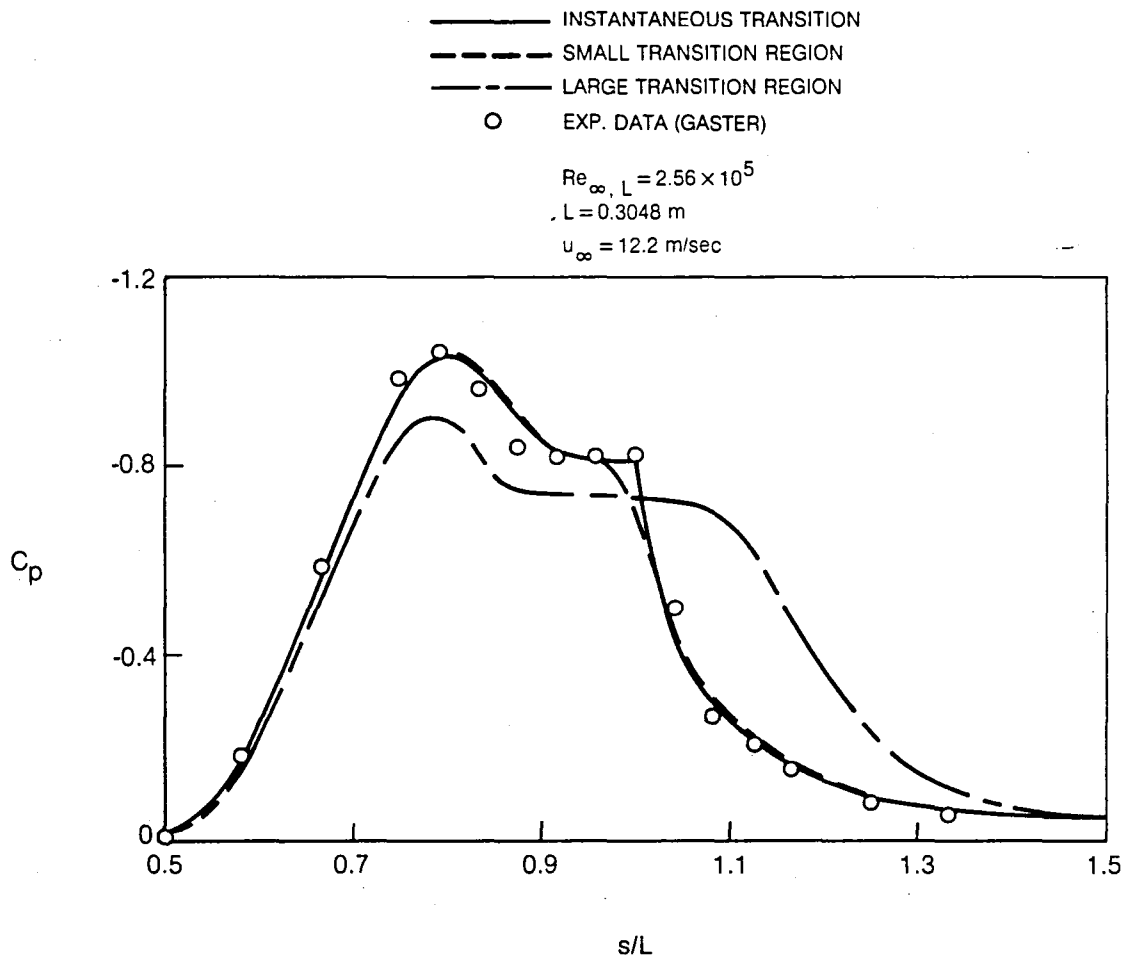

Fig. 6(b) Pressure

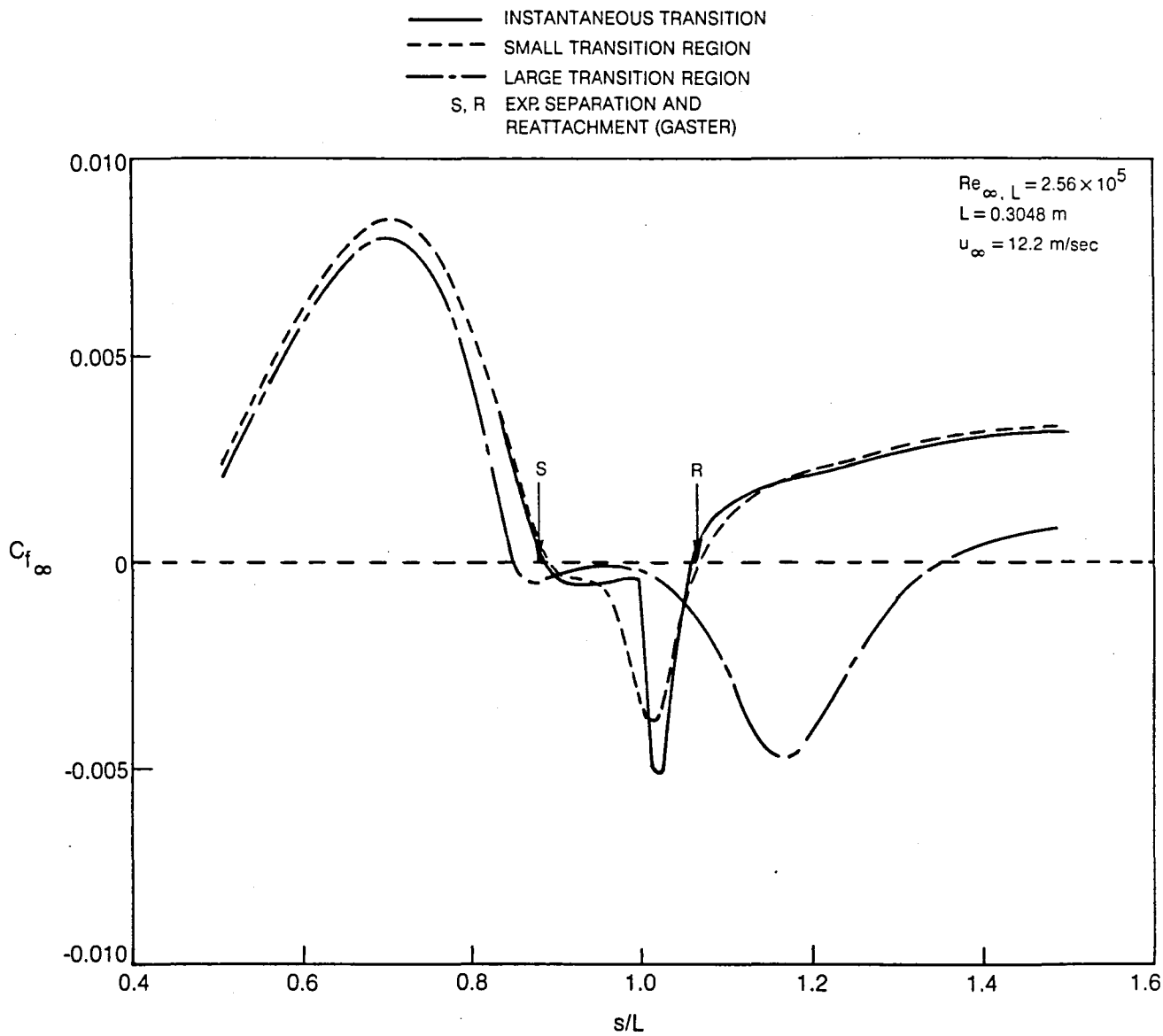

Fig. 6(c) Skin friction

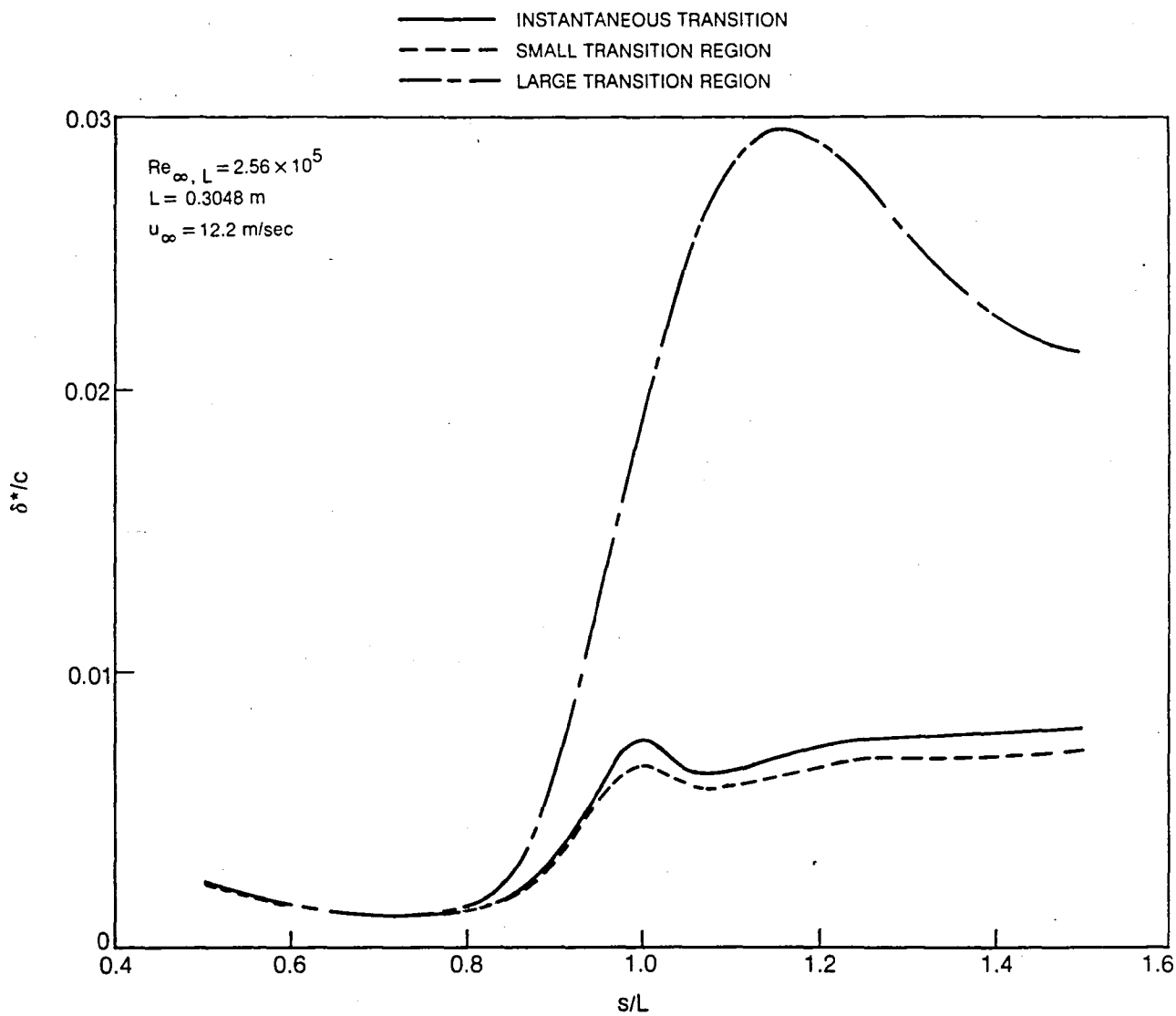

Fig. 6(d) Displacement thickness

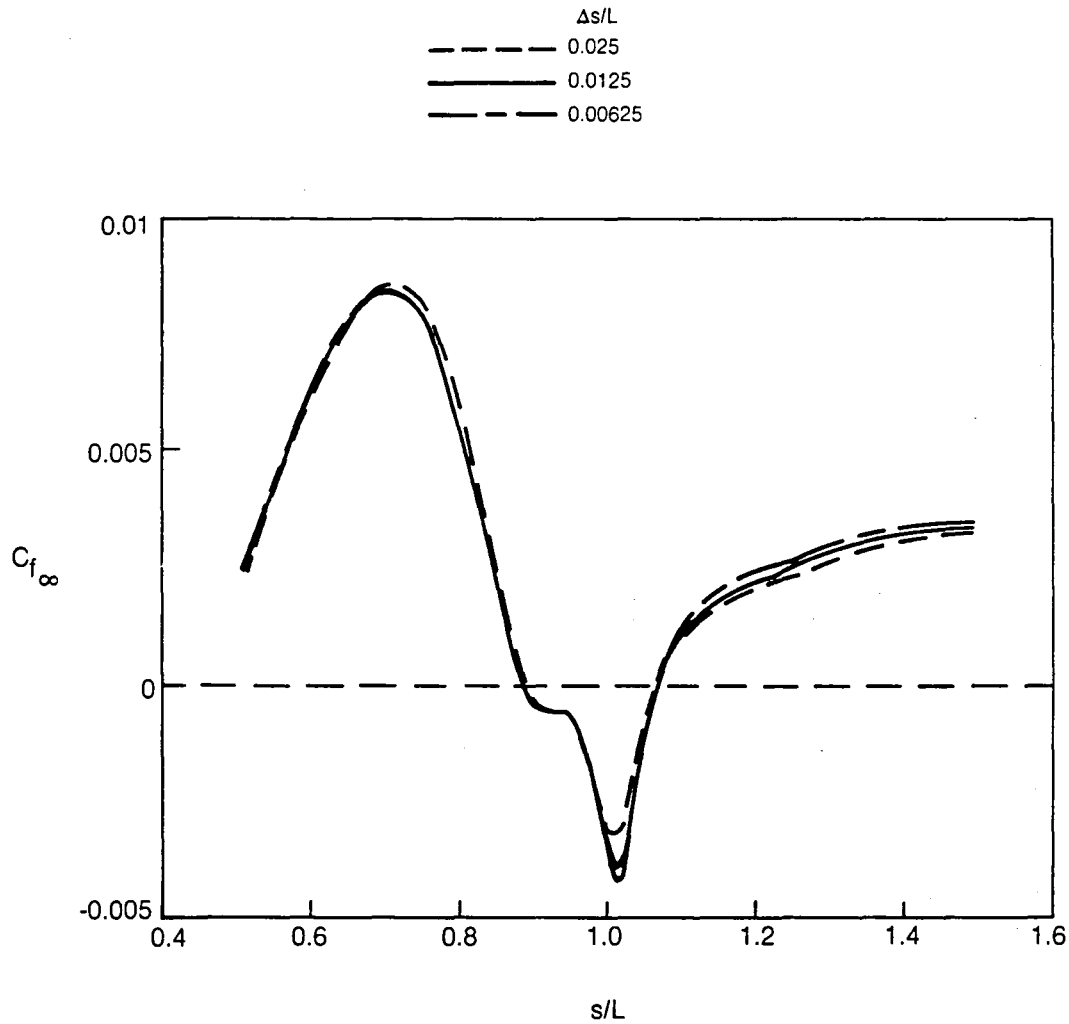

Fig. 7 Effect of streamwise mesh size on predicted results
a) Skin friction

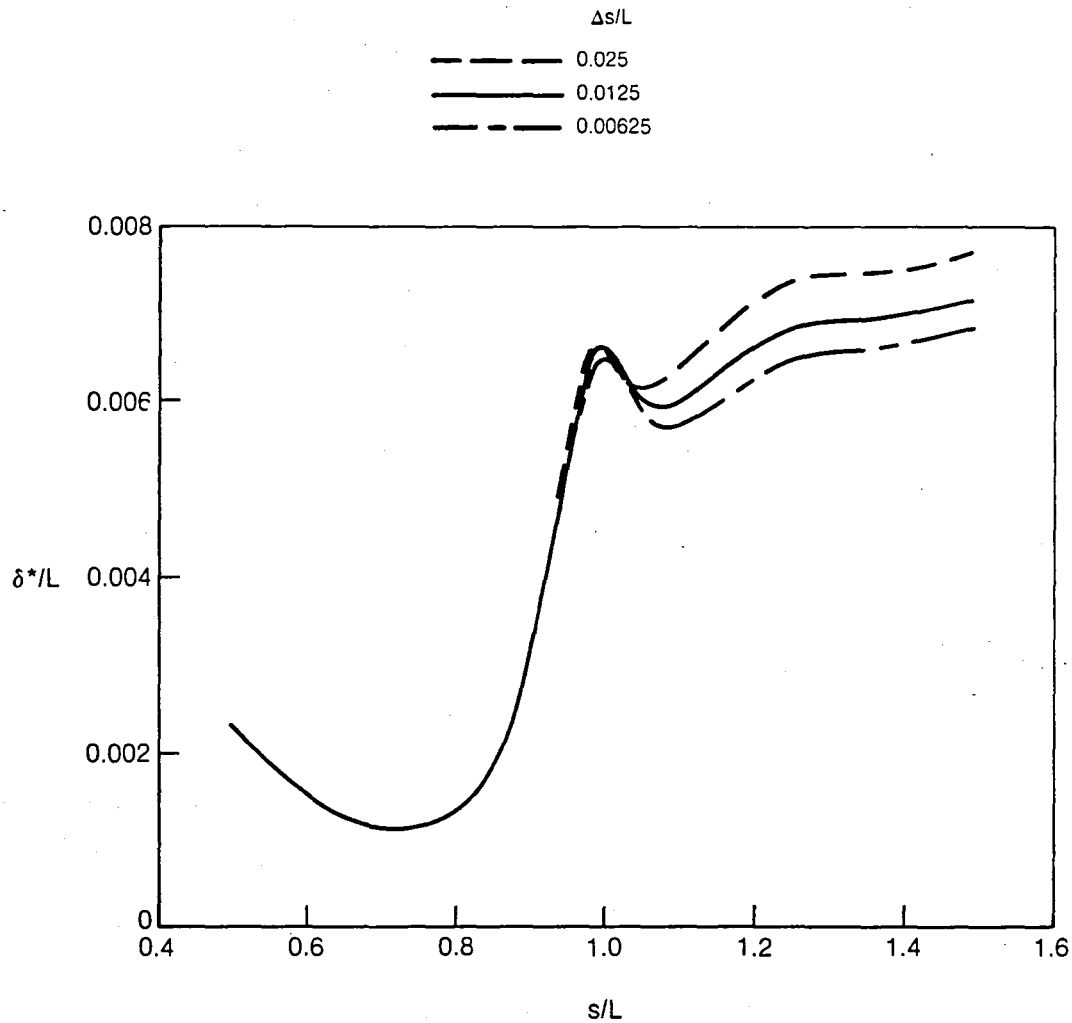

Fig. 7(b) Displacement thickness

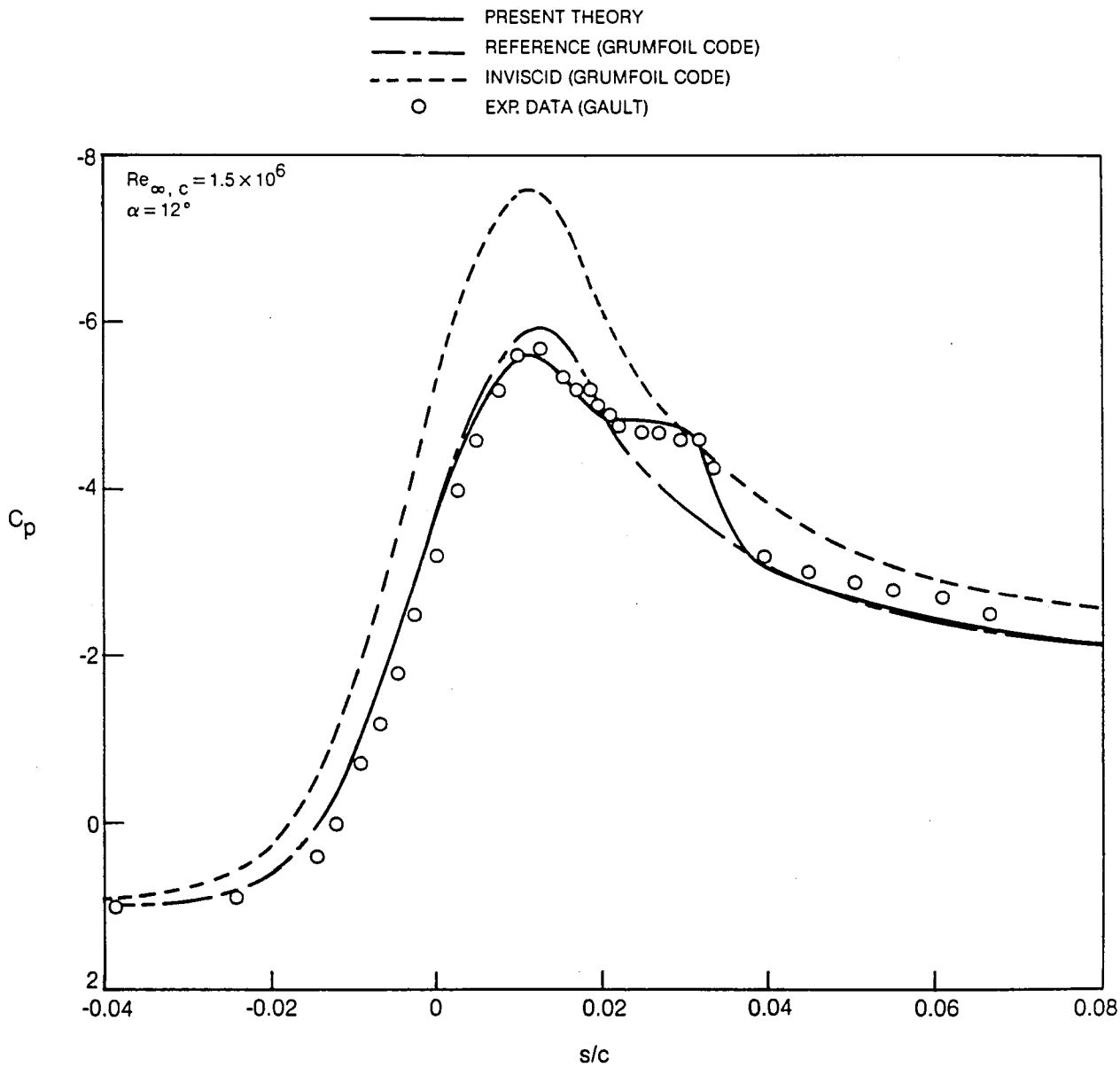

Fig. 8 Predicted results for NACA 66_3-018 airfoil
a) Pressure

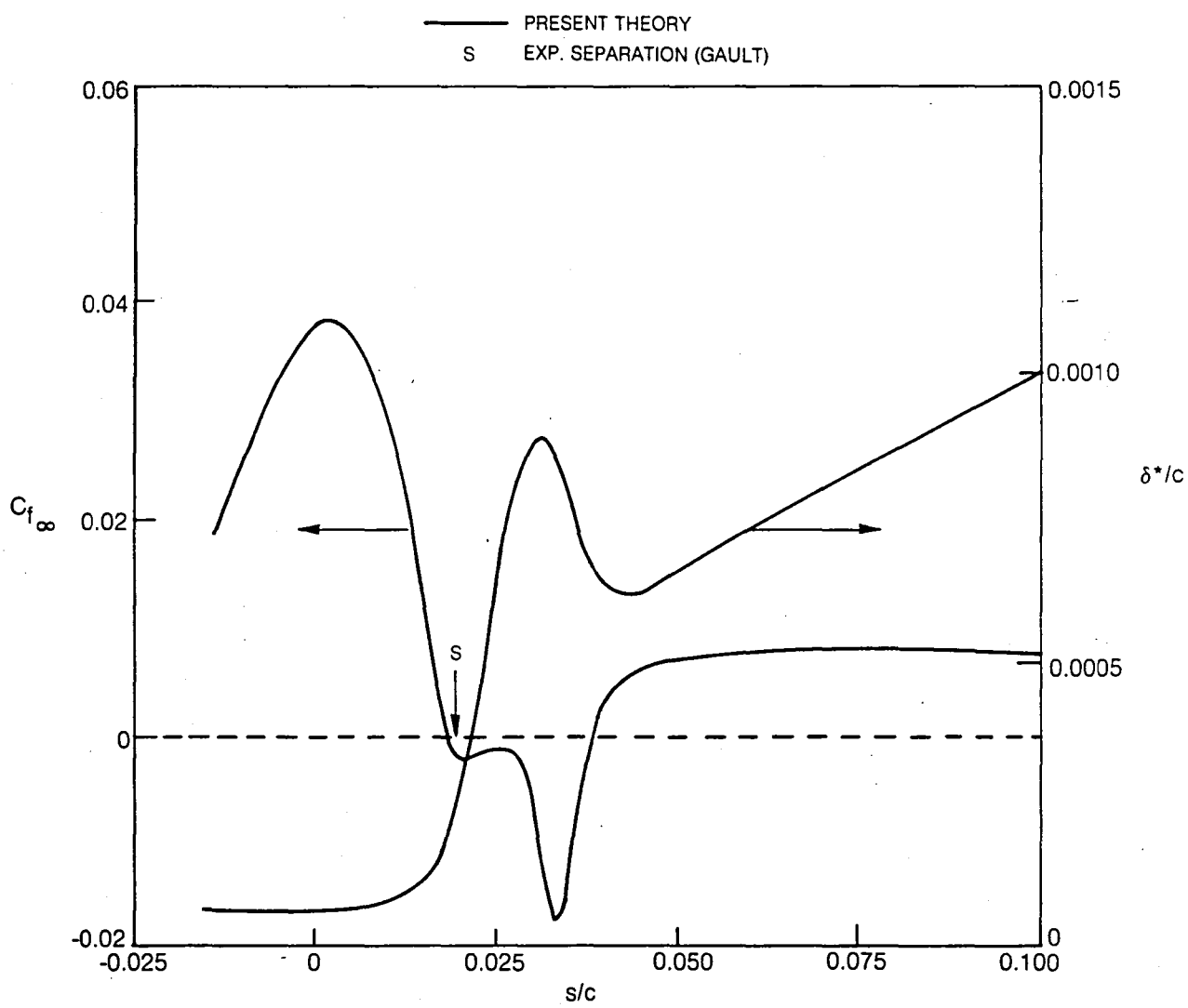

Fig. 8(b) Skin friction and displacement thickness

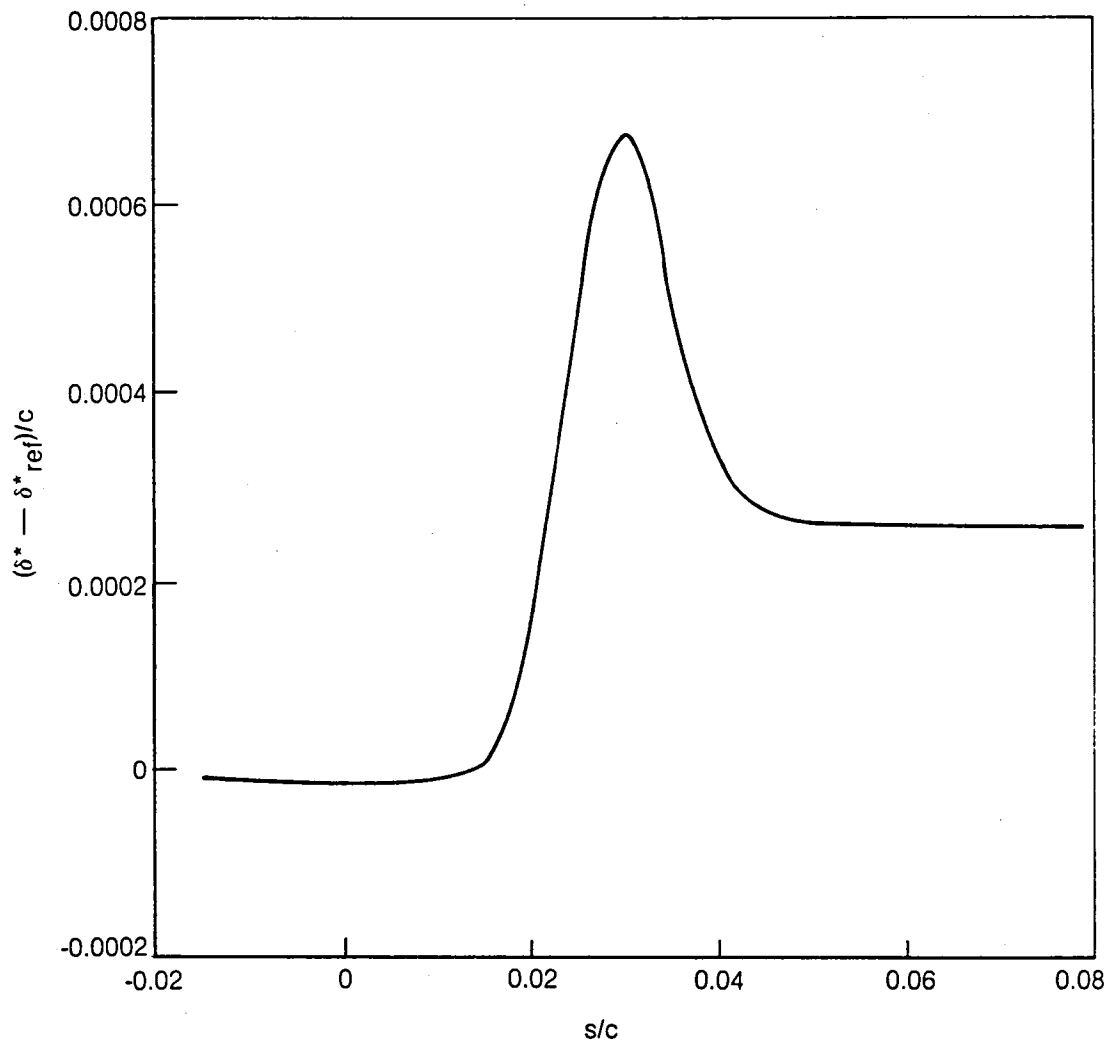

Fig. 8(c) Increment in displacement thickness due to transitional bubble

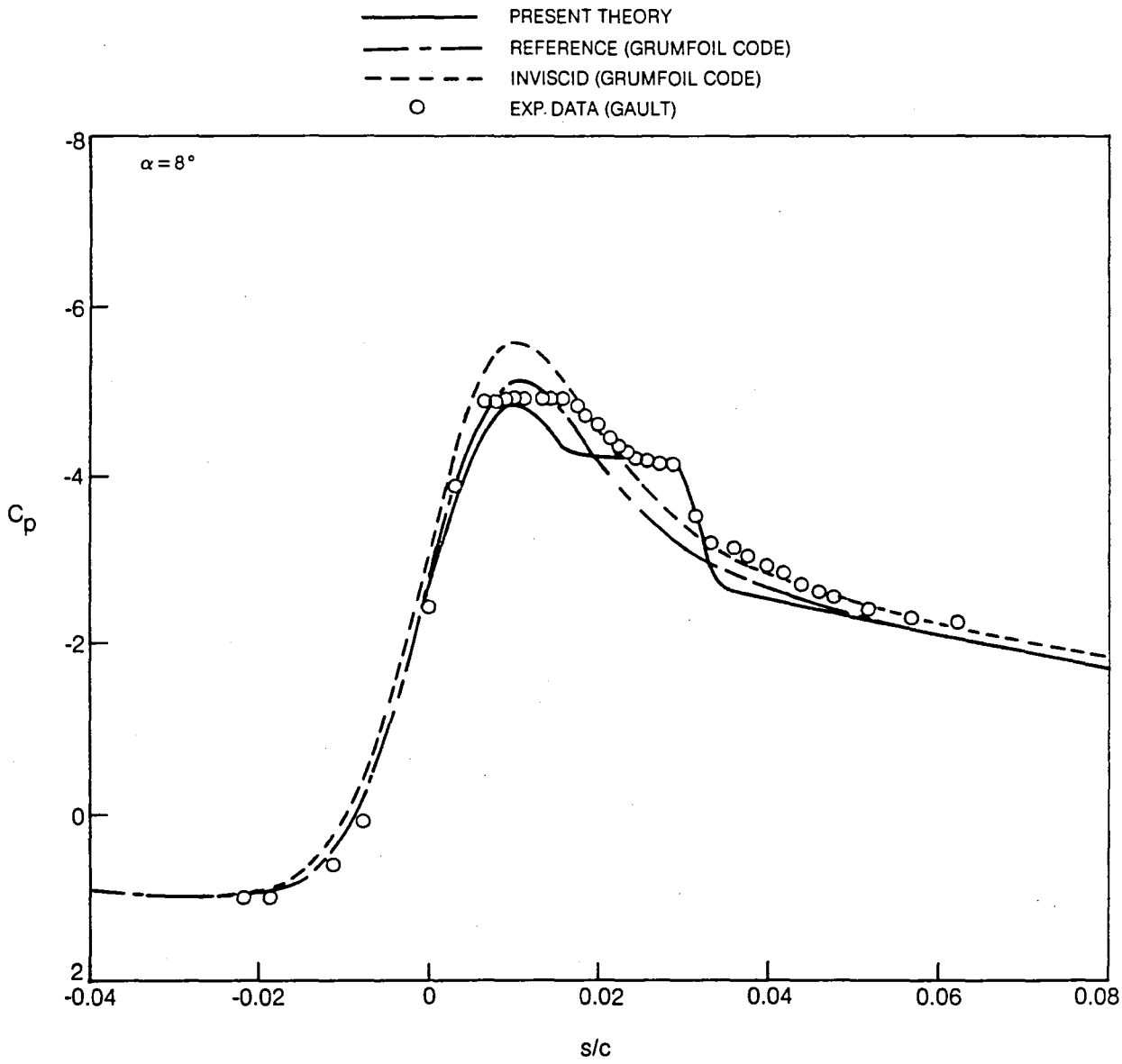

Fig. 9 Predicted results for NACA 0010 (modified) airfoil
a) Pressure distribution for $Re_{\infty,c} = 4 \times 10^6$

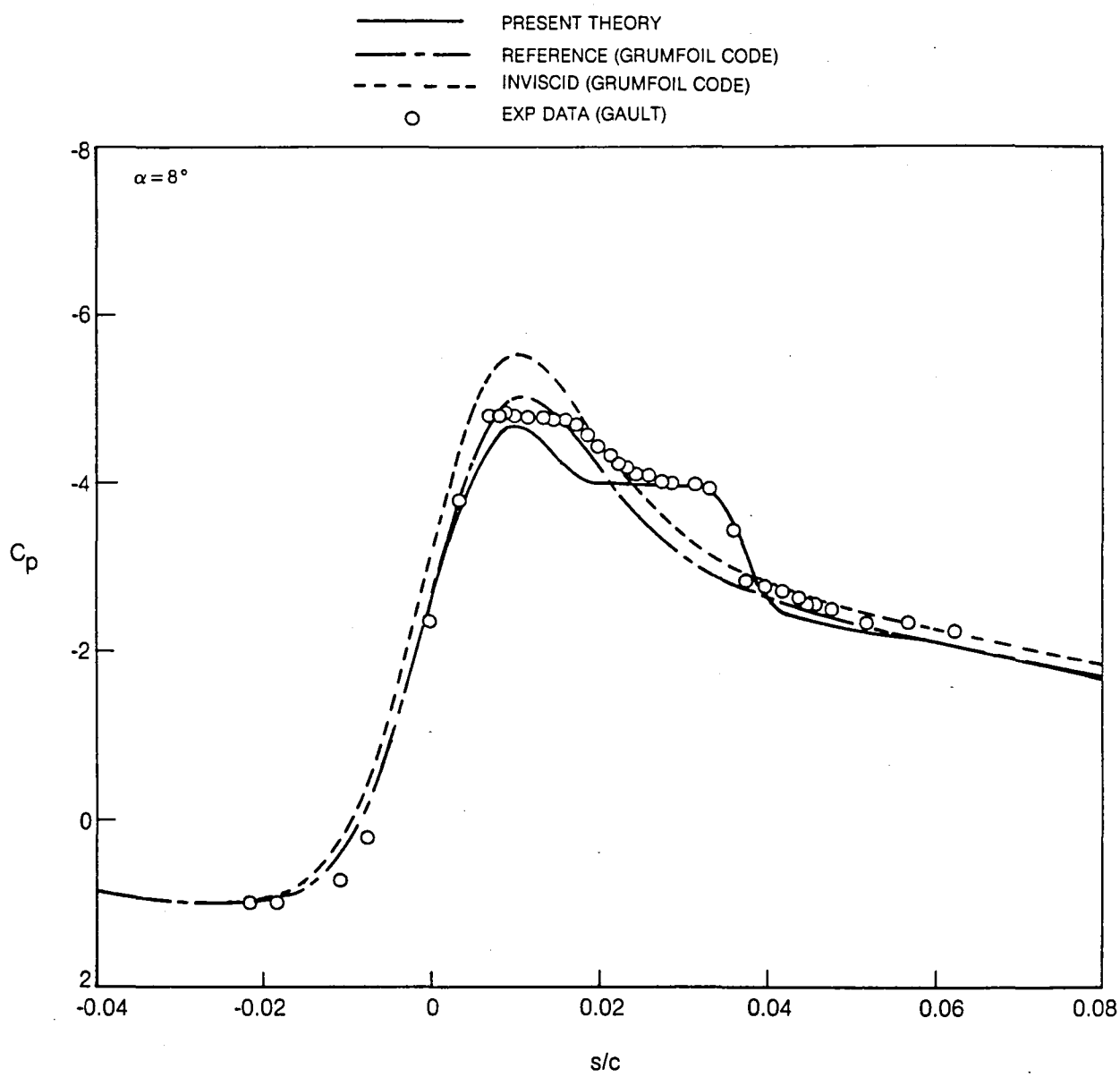

Fig. 9(b) Pressure distribution for $Re_{\infty,c} = 2 \times 10^6$

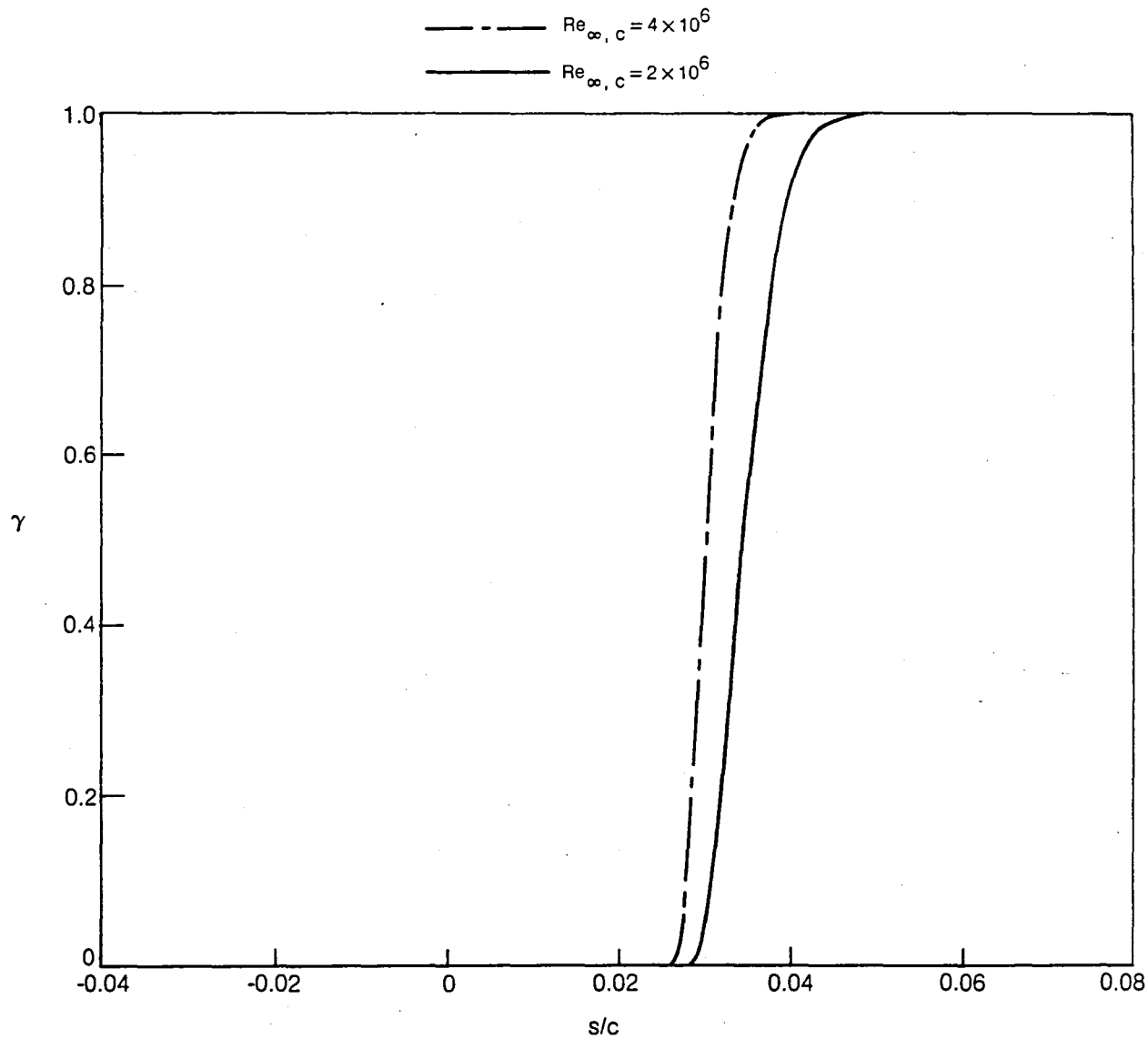

Fig. (9c) Intermittency function

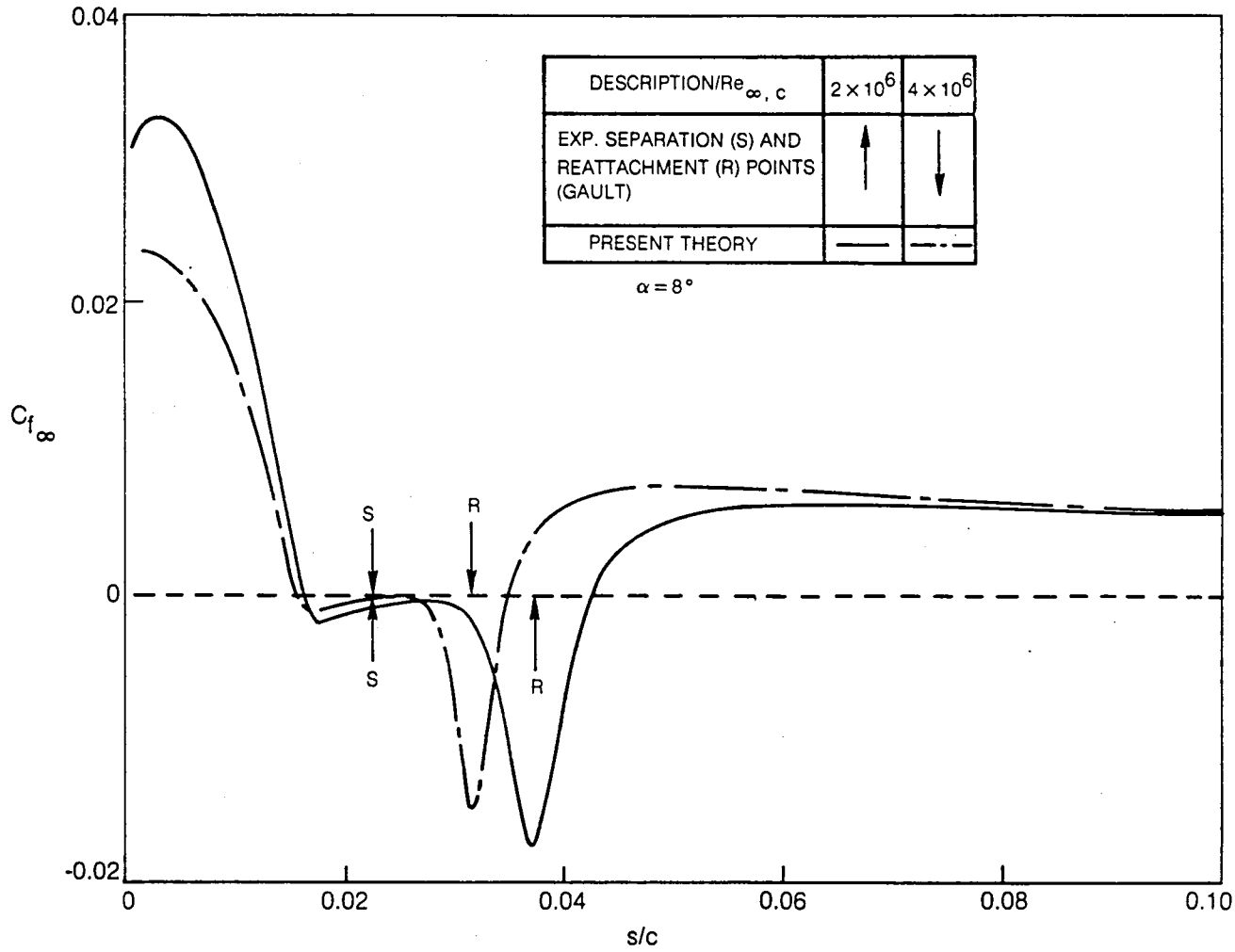

Fig. 9(d) Effect of Reynolds number on skin friction

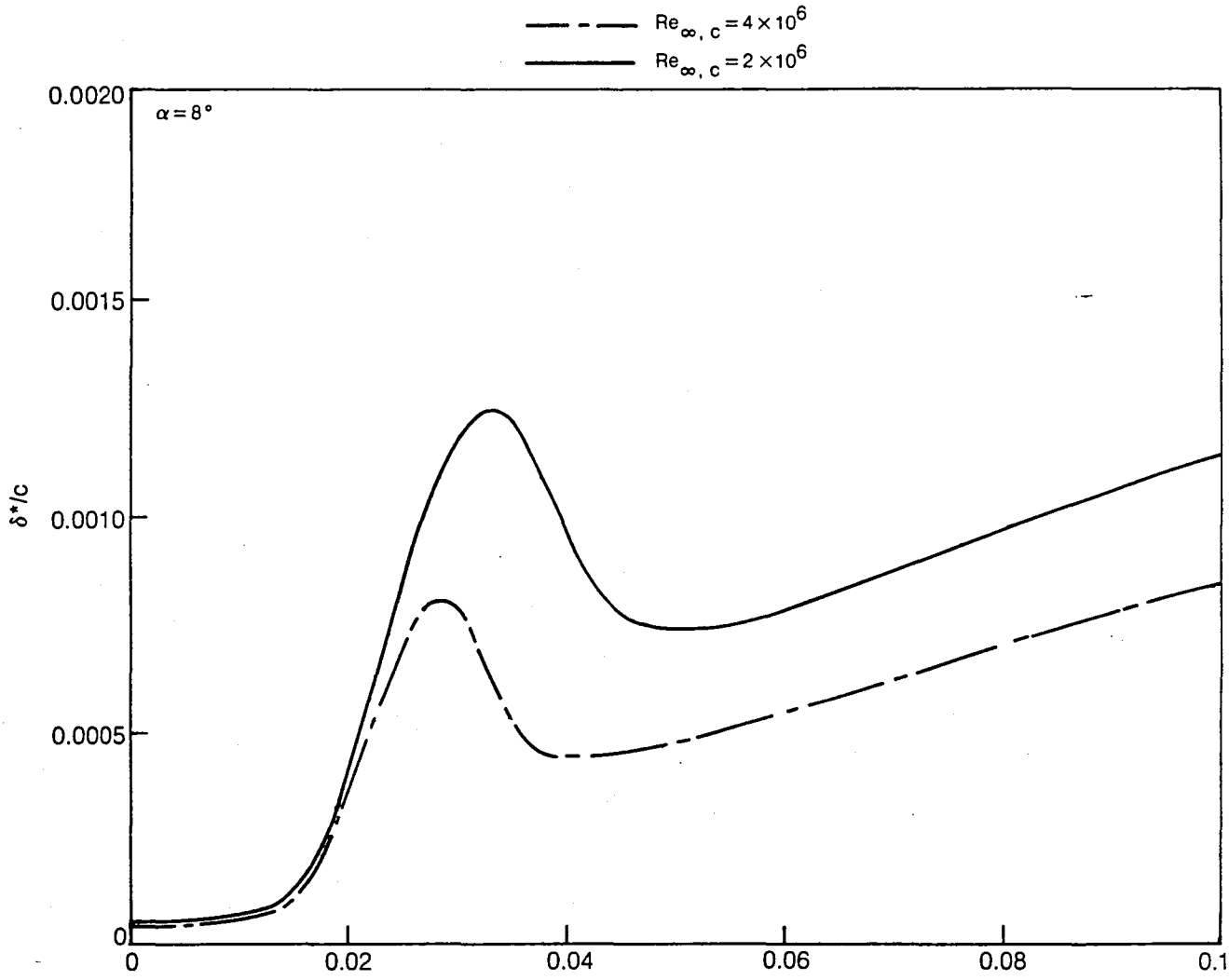

Fig. 9(e) Effect of Reynolds number on displacement thickness

1. Report No.	2. Government Accession No.	3. Recipient's Catalog No.
NASA CR-165935		

4. Title and Subtitle	5. Report Date
Analysis of Airfoil Leading Edge Separation Bubbles	May 1982
	6. Performing Organization Code

7. Author(s)	8. Performing Organization Report No.
J. E. Carter and V. N. Vatsa	R82-915622-8
	10. Work Unit No.

9. Performing Organization Name and Address	11. Contract or Grant No.
United Technologies Research Center Silver Lane East Hartford, Connecticut 06108	NAS1-16585

12. Sponsoring Agency Name and Address	13. Type of Report and Period Covered
National Aeronautics and Space Administration Washington, D.C. 20546	Contractor Report April 1, 1981-June 15, 1982
	14. Sponsoring Agency Code

15. Supplementary Notes

Langley Technical Monitor: Joel L. Everhart
Interim Report

Abstract

A local inviscid-viscous interaction technique has been developed for the analysis of low-speed airfoil leading-edge transitional separation bubbles. In this analysis an inverse boundary-layer finite-difference analysis is solved iteratively with a Cauchy integral representation of the inviscid flow which is assumed to be a linear perturbation to a known global viscous airfoil analysis. Favorable comparisons with data indicate the overall validity of the present localized interaction approach. In addition numerical tests were performed to test the sensitivity of the computed results to the mesh size, limits on the Cauchy integral, and the location of the transition region.

17. Key Words (Suggested by Author(s))	18. Distribution Statement
Airfoil, Transition, Separation, Viscous-Inviscid Interaction	Unclassified - Unlimited Subject Category 02

19. Security Classif. (of this report)	20. Security Classif. (of this page)	21. No. of Pages	22. Price*
Unclassified	Unclassified	52	

* For sale by the National Technical Information Service, Springfield, Virginia 22151

End of Document